Journal of Structural Geology 160 (2022) 104633

Contents lists available at ScienceDirect

Journal of Structural Geology

journal homepage: www.elsevier.com/locate/jsg

# Criteria to identify sedimentary sills intruded during deformation of lacustrine sequences

G.I. Alsop [a,*], R. Weinberger [b,c], S. Marco [d], T. Levi [b]

[a] Department of Geology and Geophysics, School of Geosciences, University of Aberdeen, Aberdeen, UK
[b] Geological Survey of Israel, Jerusalem, Israel
[c] Department of Geological and Environmental Sciences, Ben Gurion University of the Negev, Beer Sheva, Israel
[d] Department of Geophysics, Tel Aviv University, Israel

ARTICLE INFO

*Keywords:*
Sedimentary sill
Clastic injection
Mass transport deposit
Dead Sea Basin

ABSTRACT

Although sedimentary dykes have been widely reported across a range of settings, sedimentary sills have received somewhat less attention, perhaps due to the potential difficulties in identifying largely conformable intrusions within bedded sequences. Most outcrop descriptions of clastic intrusions are based on deep-water marine sequences, with few descriptions of sills in lacustrine settings. The recognition of sills in such settings is, however, important because lacustrine sequences are increasingly used as a record of palaeoseismic activity. The misidentification of sills that contain fragments and clasts of host stratigraphy with seismically-generated turbidites and debris flows, may lead to incorrect interpretations of palaeoseismicity. We use the Late Pleistocene Lisan Formation of the Dead Sea Basin as a case study, where laminated lake sediments preserve intricate relationships with sills. This permits us to not only establish a range of criteria used in the identification of sedimentary sills, but also examine relationships with adjacent seismically-triggered slumps and slides. Key criteria we use to recognise sills include marked changes in their thickness together with bifurcation and bridging geometries. Sills may be internally layered, contain lenses of breccia, together with aligned and folded clasts that may be truncated across upper sill contacts. Critical evidence for the interpretation of sills is also preserved along sharp but irregular upper contacts that erode and truncate bedding in the overlying host sequence. Minor apophyses and 'wedges' intrude both upwards and downwards from sills, while isoclinal recumbent 'peel-back' folds are created in host sediments by shear generated along the lower contacts of sills. We have undertaken anisotropy of magnetic susceptibility (AMS) analysis and find an oblate fabric that suggests flow and intrusion of sills along the strike of the slope, that may also help with their identification in bedded sequences. Sills form along detachments to both extensional and contractional deformation associated with seismically-generated slumps and mass transport deposits, together with sub-surface fold and thrust systems. High fluid pressures associated with injection of sedimentary sills may facilitate near-surface failure and downslope movement of the sedimentary pile.

## 1. Introduction

Although the literature has long contained numerous examples of discordant sedimentary dykes that cut across bedding and are therefore readily identified (e.g. Diller, 1890; Newsome, 1903; Jenkins, 1930) there are significantly fewer descriptions of associated sedimentary sills (for a reference list see Appendix B of Hurst et al., 2011; Levi et al., 2006b; Obermeier, 1996; Cobain et al., 2015). This may reflect the fact that distinguishing bed-parallel sedimentary sills from depositional beds is challenging, with "sills likely to be mistaken for beds" (Potter and Pettijohn, 1977, p.220), although their identification is critical to the understanding of the geology (e.g. Gao et al., 2020). The intrusion of sills into a sequence has a number of consequences for interpretations, including the raising or 'jacking up' of the overlying beds (e.g. Morley, 2003, p.391; Cobain et al., 2015, p.1818), interpretation of depositional facies (if intruded sands are not identified as such), connectivity of sands for migration of fluids and hydrocarbons (Jenkins, 1930; Dixon et al., 1995; Duranti and Hurst, 2004), and the effects of sills on mechanical stratigraphy during subsequent contractional (e.g. Palladino et al., 2016) or extensional deformation (e.g. Palladino et al., 2018).

* Corresponding author. G.I. Alsop.
*E-mail address:* ian.alsop@abdn.ac.uk (G.I. Alsop).

https://doi.org/10.1016/j.jsg.2022.104633
Received 20 March 2022; Received in revised form 13 May 2022; Accepted 18 May 2022
Available online 27 May 2022
0191-8141/© 2022 Elsevier Ltd. All rights reserved.

Many of the observations and criteria that have been established to recognise sills in sedimentary sequences are based on the intrusion of mudstone (e.g. Morley et al., 1998; Morley, 2003) and sandstone in marine and deep-water settings (see Hurst et al., 2011 for a review; Hurst et al., 2007; Cobain et al., 2015). Here we apply these criteria to shallow lacustrine settings, which are frequently used in palaeoseismic studies, as lakes are widespread and provide a refined stratigraphic template that readily records sediment movement associated with large earthquakes (e.g. Gao et al., 2020). In addition, some of the other potential triggers of soft-sediment deformation (SSD) associated with sedimentary dykes and sills, such as storm waves and tides, can be discounted in lacustrine settings due to the limited size of water bodies (e.g. Gao et al., 2020). Previous studies that have identified minor sedimentary sills associated with SSD in lacustrine settings include Törő and Pratt (2015a, b, 2016) and Gao et al. (2020), although sills have in general not been widely-reported from such settings. An understanding of sedimentary sills that are injected into the lacustrine stratigraphy is, however, critical for the use of such sequences in palaeoseismic studies, as mobilised sediment and sills may easily be overlooked or confused with depositional units in the bedded sediments. It is crucial to distinguish sills from turbidites and debris flows, as these units are often used to constrain surficial SSD and hence earthquake timing in palaeoseismic studies (e.g. Lu et al., 2017, 2021a, b, c). Our aim is therefore to provide a first detailed account of criteria that may be used to distinguish sedimentary sills in lacustrine settings. This study addresses a number of research questions relating to sedimentary sills and their relationship with gravity-driven deformation including:

a) What controls the location of sills?
b) Is deformation associated with intrusion of sills?
c) How are folded clasts created within sills?
d) Which criteria help identify bed-parallel sills?
e) What is the timing and role of sills in gravity-driven deformation?
f) What are the consequences of mis-identifying sills?

### 1.1. Sediment mobilization and soft-sediment deformation

Increases in pore fluid pressure are an effective mechanism to reduce the shear strength of sediments and thereby expedite their failure (e.g. Maltman, 1994a, b and references therein). Although pore fluid pressures within sediments may be increased by a wide range of factors (see Obermeier, 1996, 2009 for reviews) one of the most widely-cited triggers are earthquake events. Seismicity may trigger the initial slope failure that creates a slump sheet or mass transport deposit (MTD) that then translates downslope under the influence of gravity. Thicker slumped units may locally increase the loading and pore fluid pressures on underlying sediments, potentially leading to the injection of sedimentary intrusions, thereby promoting continued downslope translation (e.g. Strachan, 2002).

In general, the mobilization of unlithified sediments is defined as "rendering the sediment capable of motion and the bulk movement that commonly results" (Maltman and Bolton, 2003, p.9). The nature of the structures that form in unlithified sediment are determined by relationships between the ratio of the cohesive strength of the sediment (due to grain weight) and the pore fluid pressure (Knipe, 1986; Ortner, 2007). Fluid pressure lower than grain weight generates hydroplastic deformation that modifies bedding to create folds and shears. When fluid pressure is equal to grain weight, then sediment liquefies to form laminar flow and bedding is destroyed. Finally, when fluid pressure is greater than grain weight, sediment fluidization occurs and generates turbulent flow that carries grains and destroys bedding (Knipe, 1986). Liquidization (including liquefaction) is a form of independent particulate flow (Knipe, 1986) and results in grains temporarily losing contact with one another, thereby permitting relative rotation and translation between grains.

### 1.2. Methodology of AMS analysis in sedimentary sills

Deformation within rocks and sediments is characterised by magnetic fabrics which are analysed via the anisotropy of magnetic susceptibility (AMS) (e.g. Parés, 2015). The AMS analysis is commonly used for depicting petrofabrics in soft sediments, revealing the flow and MTDs transport directions (e.g. Weinberger et al., 2017 and references therein) and quantifying inelastic deformation (e.g. Schwehr and Tauxe, 2003; Borradaile and Jackson, 2004; Levi et al., 2018; Weinberger et al., 2017, 2022). In this study we apply AMS analysis in order to characterize the magnetic fabric of sedimentary sills and thereby potentially recognise the direction of sediment injection.

AMS is a second-rank tensor which is described by its principal values and principal axes, which are commonly represented as an ellipsoid (Borradaile and Jackson, 2004). The $k_1$, $k_2$ and $k_3$ eigenvalues of the AMS correlate with the maximum $K_1$, intermediate $K_2$ and minimum $K_3$ magnetic susceptibility axes. The long and short axes of particle shapes are generally aligned parallel to the maximum ($K_1$) and minimum ($K_3$) axes of magnetic susceptibility. Elongate particles deposited in still-water tend to lie parallel to the horizontal bedding plane, thereby creating a 'deposition fabric'. This is marked by vertical and well-clustered $K_3$ axes, while $K_1$ and $K_2$ axes are somewhat distinguishable and lie within the bedding plane forming an oblate shape to the AMS ellipsoid ($k_3 \ll k_1$, $k_2$) (see Levi et al., 2006b). The original deposition magnetic fabric might evolve into a 'deformation fabric' or 'injection fabric' during later soft-sediment deformation, in which the $K_1$ and $K_2$ axes are well-clustered and clearly distinguishable.

The AMS in the case study was measured using a *KLY-4S* Kappabridge (AGICO Inc.) at the Geological Survey of Israel rock-magnetic laboratory, where the principal susceptibility axes and their 95% confidence ellipses (Jelinek 1978) were analysed with *Anisoft42*. Mean susceptibility ($k_m = k_1 + k_2 + k_3/3$), degree of anisotropy ($P = k_1/k_3$) and shape of the AMS ($T = (2\ln k_2 - \ln k_1 - \ln k_3)/(\ln k_1 - \ln k_3)$), were calculated according to Jelínek (1981) and Tarling and Hrouda (1993).

### 1.3. Injection of sedimentary sills

It has long been recognised that sandstone dykes and sills are "the result of the forcible intrusion of liquified sand into a cohesive host" (Collinson, 1994, p.111). Sills are considered to fill and inject along natural hydraulic fractures that largely propagate along weaker bedding planes and open normal to the plane of least compression (see Cobain et al., 2015 for a recent summary) (Fig. 1). It is also considered that sills are intruded at shallow depths "where the vertical pore-fluid pressure gradient is equal to, or exceeds the overburden pressure, resulting in the minimum principal stress (σ3) being vertical" (Palladino et al., 2020, p.14 and references therein) (Fig. 1).

When considering sedimentary sills, it should be appreciated that they differ from igneous sills in that they may be locally mobilised and entirely sourced from immediately adjacent sediment, whereas igneous intrusions generally emanate from greater depths. Intrastratal deformation horizons created by the lateral flow and injection of sediment may evolve laterally into sills, although it should be noted that the two features "do not present a clear or essential distinction" (Kawakami and Kawamura (2002, p.178) (Fig. 1). This point was summarised by Ogawa (2019, p.12) who states that "coherent beds are transitionally liquefied and intruding along the same horizon as sills, or remain at the same horizon as in situ brecciated beds". Thus, some susceptible beds may laterally evolve into horizons of locally mobilised sediment and sills that broadly maintain the same stratigraphic level (Fig. 1). This is considered a consequence of the injected sill failing to achieve a great enough fluid pressure that would permit it to overcome the strength of the overlying strata (Ogawa, 2019, p.12).

A number of key papers have attempted to define detailed outcrop-based criteria that may be used to identify sandstone sills in basinal marine settings, and include Hiscott (1979), Archer (1984), Kawakami

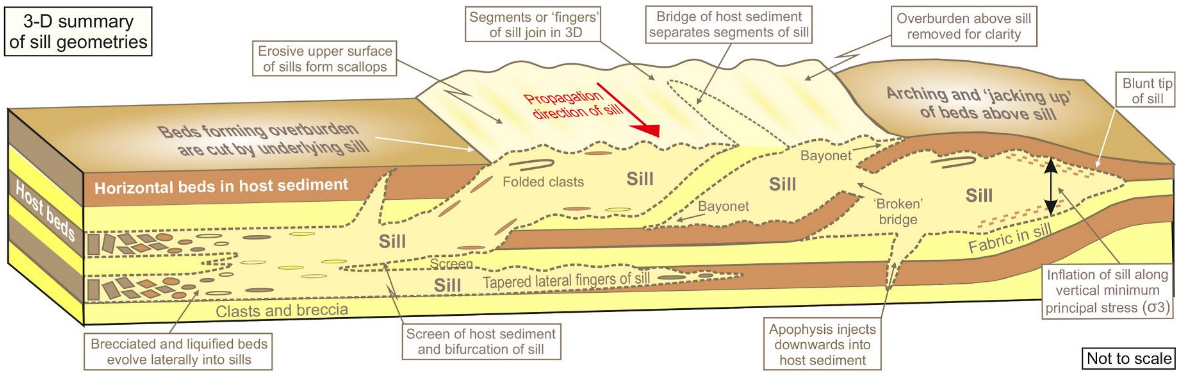


**Fig. 1.** Cartoon highlighting some generalized features of a sedimentary sill injected towards the viewer into a bedded sequence. Brecciated and liquified beds evolve laterally into sills that bifurcate and segment as they intrude across the layered sequence resulting in local uplift and 'jacking-up' of overlying beds. Bridges separate segments of the sill that amalgamate and join in 3-D with local erosion and cross-cutting of overlying host strata.

and Kawamura (2002), Macdonald and Flecker (2007), Hurst et al. (2011) and Palladino et al. (2020). Using the Dead Sea Basin as our case study, we utilise this range of criteria established in marine environments and apply them to sedimentary sills formed in a lacustrine setting.

## 2. Geological setting

### 2.1. Regional geology

The Dead Sea Basin is a continental depression bound by the western border fault zone, which comprises a series of oblique-normal stepped faults, and the left-lateral eastern border fault (Fig. 2a and b) (Marco et al., 1996, 2003; Ken-Tor et al., 2001; Migowski et al., 2004; Begin et al., 2005). These faults comprise the Dead Sea Fault (DSF) system that was active from the Early Miocene to Recent (Nuriel et al., 2017), and has generated numerous earthquakes leading to deformation of the basin-fill deposits. The present study focusses on the Late Pleistocene Lisan Formation that was deposited in Lake Lisan at 70–14 ka and forms a pre-cursor to the modern Dead Sea (e.g. Haase-Schramm et al., 2004). The Lisan Formation comprises mm-scale aragonite laminae that were precipitated from the hypersaline waters of Lake Lisan during the summer, while sporadic flood events washed detrital-rich layers into the lake during the winter (Begin et al., 1974; Ben-Dor et al., 2019). Thin detrital laminae display grain sizes of ~8–10 μm (silt), while the thicker (>10 cm) detrital-rich beds deposited after major floods comprise very fine (60–70 μm) sands (Haliva-Cohen et al., 2012). The detrital units are composed of quartz and calcite grains with minor feldspar and clays (illite-smectite) (Haliva-Cohen et al., 2012). Counting of aragonite-detrital varves, bracketed by isotopic dating, indicates average depositional rates of ~1 mm per year for the Lisan Formation (Prasad et al., 2009).

### 2.2. Patterns of slope failure around the basin

The Lisan Formation preserves very low <1° depositional dips that are directed towards the depocentre of the Dead Sea Basin. Seismically-induced slope failure leads to downslope movement of sediment resulting in MTDs that form at the surface (e.g. Alsop et al., 2020d), together with potentially deeper sub-surface fold and thrust systems (FATS) and bed-parallel slip (BPS) planes (e.g. Alsop et al., 2020a, 2021a, b). Major earthquakes may also result in overturn and mixing of the water column that leads to precipitation of relatively competent 1 m thick gypsum horizons within the Lisan Formation (Ichinose and Begin, 2004; Begin et al., 2005). At the time of seismically-triggered deformation, the Lisan Formation is considered to have been weak and fluid saturated, and still currently retains ~25% fluid content (Arkin and Michaeli, 1986; Frydman et al., 2008).

The gravity-driven structures combine to create a regional pattern of radial slumping linked to the transfer of sediment downslope towards the depocentre of the basin (Alsop et al., 2020d) (Fig. 2a and b). Thus, in the northern part of the basin, the Lisan Formation displays SE-directed slumping, the central portion shows E-directed MTDs, the southern basin at Peratzim is marked by NE-directed slumping, while westerly-directed movement has been recorded from the eastern shores of the Dead Sea in Jordan (El-Isa and Mustafa, 1986) (Fig. 2b). Magnetic fabrics confirm the directions of slumping (Weinberger et al., 2017), with the bulk movement of sediment from the basin margins towards the centre resulting in the Lisan Formation being three times thicker in the depocenter, where drill cores penetrate numerous MTDs (Lu et al., 2017, 2021a, b, c; Kagan et al., 2018).

### 2.3. Rationale for study area

The varve-like laminae of the Lisan Formation preserve detailed structural and stratigraphic relationships, making the Dead Sea Basin an ideal place to study the intrusion of sedimentary sills. Regional slopes that are visible today provide a clear kinematic framework, while the finely laminated upper 'White Cliff' portion of the Lisan Formation (Bartov et al., 2002) that was deposited at 31–15 ka (Torfstein et al., 2013) provides the best sections for analysis of sills. The Lisan Formation contains a range of deformed horizons that formed at varying depths below the surface:

a) Surficial deformation created MTDs that are directly overlain by sedimentary caps deposited out of suspension immediately following the slope failure (Alsop et al., 2018; 2020d).
b) Shallowly buried (<1 m) deformation created FATS bound by upper and lower detachments that directly influence overlying sedimentation at the surface (Alsop et al., 2021a, 2022).
c) Buried deformation at depths of up to 20 m below the surface (the thickness of the hosting White Cliff strata) that created intrastratal FATS and BPS detachments (Alsop et al., 2020a, 2022).
d) Buried deformation at depths of up to 20 m below the surface that created horizontal BPS marked by 2–10 mm thick layers of gouge formed during co-seismic shaking (Weinberger et al., 2016).

The Lisan Formation therefore presents an opportunity to study the interaction of sedimentary sills with a range of deformation styles and depths below the surface in a lacustrine setting. Sills were intruded at maximum depths below the sediment surface of 20 m (the thickness of the hosting strata) and more generally <10 m. The interaction of some sills with surficial MTDs suggests very shallow intrusion within a few metres of the depositional surface on the lake floor. We take our examples of sills from two sites within the Lisan Formation at Miflat

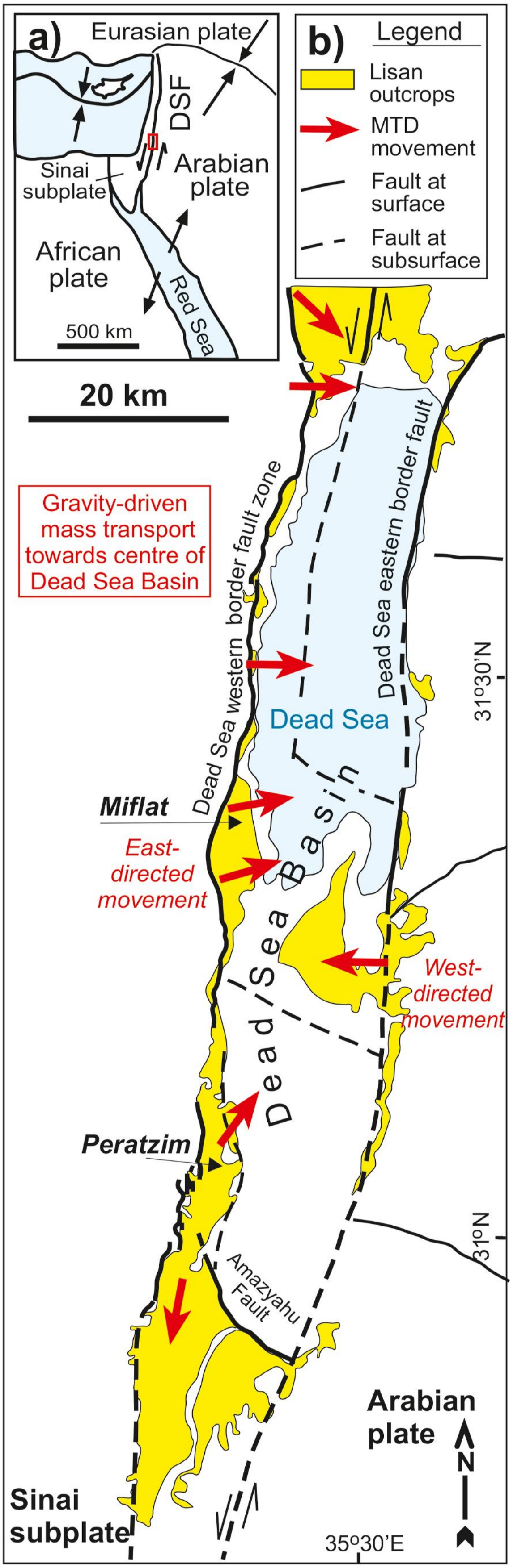


(caption on next column)

**Fig. 2.** a) Tectonic plates in the Middle East. General tectonic map showing the location of the present Dead Sea Fault (DSF), which transfers the opening motion in the Red Sea to the Taurus-Zagros collision zone. Red box marks the study area in the Dead Sea Basin. b) Generalized map (based on Sneh and Weinberger, 2014) showing the current Dead Sea including the position of the Miflat and Peratzim localities referred to in the text. The extent of the Lisan Formation outcrops is also shown, together with the general fold and thrust system directions of the MTDs around the basin. (For interpretation of the references to colour in this figure legend, the reader is referred to the Web version of this article.)

[N31°:21.42″ E35°:22.49’’] and Peratzim [N31°:04.56″ E35°:21.02’’] (Fig. 2b). These sites are located ~1–2 km east of Cenomanian-Senonian carbonates that form the footwall of the Dead Sea western border fault zone and represent marginal areas to Lake Lisan (Fig. 2b). Estimated water depths in Lake Lisan at these sites are <100 m from 70 to 28 ka, and up to 200 m water depth between 26–24 ka (Bartov et al., 2002, 2003).

### 2.4. Deformation, sedimentary sills and post-slumping clastic dykes

Modern flash floods sporadically incise wadis through the Lisan Formation creating vertical sections parallel to the movement direction of earlier gravity-driven failures (Alsop et al., 2017; 2020d). Although some variability exists, slump fold hinges typically trend NW-SE and verge towards the depocentre of the basin further to the NE (Alsop et al., 2021a) (Fig. 2b). At Miflat, fold hinges are NNW-SSE trending with slump transport directed towards the ENE and the centre of the basin (Alsop et al., 2020a) (Fig. 2b). Previous analysis of slump folds using dip isogons (e.g. see Ramsay, 1967; Fossen, 2016, p.225 for details of the technique) shows folded aragonite layers to display Class 2 fold styles, whereas detrital-rich layers are marked by more parallel (Class 1) folds (Alsop et al., 2020c). This suggests that, at the time of folding, aragonite layers were weaker than the detrital beds, which were generally thicker and more competent (Alsop et al., 2017; 2020c).

The gravity-driven deformation noted above and in previous publications (e.g. Alsop et al., 2019) was seismically-triggered and is associated with previously undescribed sedimentary sills in the Lisan Formation. Sills are generally less than 0.5 m thick and comprise a mixture of disaggregated fine-grained sand and silt aragonite and detrital grains that are mixed together to form a brown or buff-coloured sediment. The colour variation of the matrix is interpreted to reflect varying components of aragonite and detrital grains and is similar to gouge created along thrusts and detachments (e.g. Weinberger et al., 2016; Alsop et al., 2018). Larger (up to 10 cm) aragonite and detrital fragments are preserved within the finer matrix of sills and show local fracturing and disaggregation. The lack of compaction-related fabrics reflects the absence of appreciable overburden (<10 m), suggesting only limited later compaction occurred (see Alsop et al., 2019).

The sedimentary sills, together with the various types of gravity-driven structures (MTDs, FATS, BPS), are subsequently cut across by clastic dykes which were triggered by seismicity and are a widespread feature in the Lisan Formation (e.g. Levi et al., 2006a, b). The late-stage clastic dykes locally feed minor sedimentary sills that formed up to 18 m below the depositional surface (Levi et al., 2006b), but these younger intrusions are unrelated and cut across the older MTDs and sedimentary sills that we describe here.

Optically stimulated luminescence (OSL) dates on sediment contained within the late-stage dykes gives ages of between 15 and 7 ka (Porat et al., 2007) and they therefore post-date deposition and associated gravity-driven deformation of the upper White Cliff Lisan Formation at 31–15 ka (Haase-Schramm et al., 2004; Torfstein et al., 2013). The clastic dykes may themselves be locally offset by subsequent co-seismic horizontal slip (Weinberger et al., 2016) but are otherwise undeformed and show no evidence of vertical shortening linked to compaction. We now provide examples of some of the key features that are used to identify sedimentary sills in bedded lacustrine sequences from the Lisan Formation. In all photographs, the eastern (downslope) side is on the right, while scale is provided by a 15 mm diameter coin, 10 cm chequered rule, and a 30 cm long hammer.

## 3. External geometry of sills

The overall geometry of sedimentary intrusions provides a range of basic features and relationships described below that may be used to help determine the nature and origin of sills.

### 3.1. Changes in thickness of sills

The geometry of sedimentary sills has been previously mapped in detail by Hiscott (1979) and described by Archer (1984) who note that sills may laterally terminate in a range of steep and 'blunt' margins, (e.g. Palladino et al., 2020, p.5) or may display more tapered shapes (Fig. 1). These more tapered terminations have been described as overall

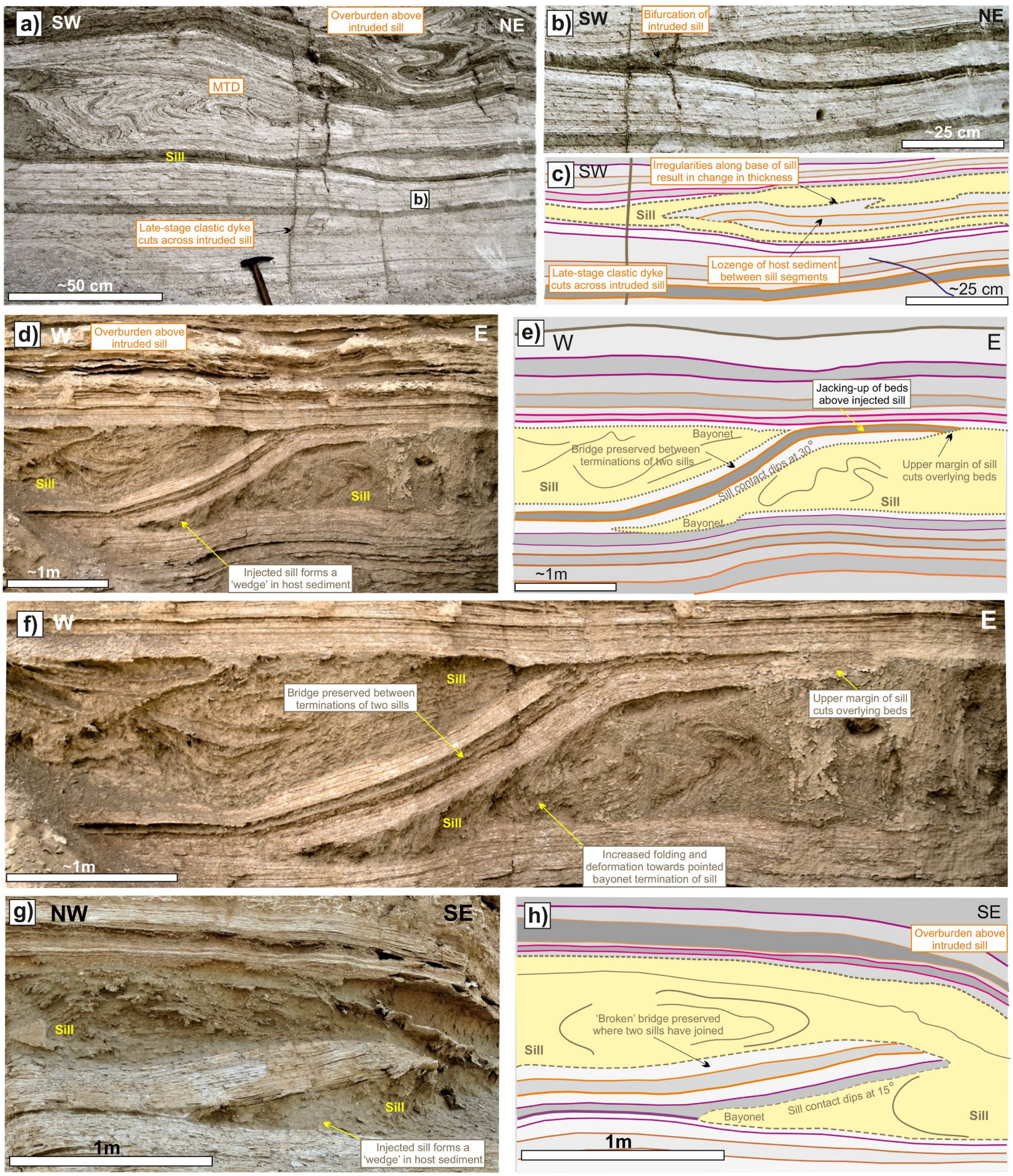


**Fig. 3.** a) Bifurcating detritus-rich sill with b) close-up photograph and c) associated line drawing highlighting the gently cross-cutting geometry of the sill (Peratzim). The sill is overlain by a mass transport deposit (MTD) and is cross-cut by a late-stage clastic dyke. d) Photograph and e) line drawing of a sediment bridge that dips at 30° and is positioned below the western sill segment and above the eastern segment (Miflat). f) Close-up photograph of the bridge that displays uniform stratigraphic thickness, while the lateral termination of each segment is marked by a pointed 'bayonet' geometry. g) Photograph and h) associated line drawing of a 'broken bridge' dipping at 15° and underlain by a pointed wedge or termination to a sill (Miflat). Two segments of sills are considered to have broken through the bridge and amalgamated.

wedge-shaped geometries (Kawakami and Kawamura, 2002, p.172).

In new examples from the case study, we observe irregularities in the lower contact of sills that are associated with rapid and significant changes in thickness of the sill (Fig. 3a–c). The changes in thickness are locally pronounced with sills more than doubling in thickness over relatively short (25 cm) distances (Fig. 3a–c).

### 3.2. Bifurcation and bridging in sills

The lateral bifurcation of sedimentary sills has been previously shown and described by Truswell (1972), Hiscott (1979), Archer (1984) Parize and Fries (2003), and Macdonald and Flecker (2007) (Fig. 1).

In new examples from the case study, bifurcation of sills results in two fingers of injected sediment intruding into weaker aragonite-rich beds (Fig. 3a–c). A lozenge of host stratigraphy is preserved between the two intrusions (Fig. 3a–c). In some cases, distinct beds of aragonite-rich stratigraphy dipping at 30° separate two pointed terminations of sill segments that form 'bayonet' features (Figs. 1, 3d-f). The screen or 'bridge' of sediment between the two segments of the sill is beneath one segment and above the other and does not therefore correspond to a thrust configuration. The bridge may remain relatively intact and separate the two sill segments (Fig. 3d–f) or be compromised such that the 'broken bridge' protrudes into the amalgamated sill (Figs. 1 and 3g, h). These features are similar to those observed previously in sedimentary sills (e.g. Archer, 1984, p.1201) and also more generally in igneous sills (e.g. Baer, 1993; Hutton, 2009; Magee et al., 2019) (Fig. 1).

### 3.3. Screens of host sediment

Thin (<5 cm) laterally continuous, laminated layers that have the same appearance as the adjacent host sediments are preserved within deformed and injected sedimentary horizons (Kawakami and Kawamura, 2002, p.175) (Fig. 1). Screens also separate the 'multi-layer' sills previously described by Hurst et al. (2011, p.222).

Within the case study, we observe comparable thin (<2 cm) laminated layers within sills, which are interpreted as 'screens' of host sediment parallel to the margins of the sill (Fig. 4a–k). These thin horizons display injection and wedging by the overlying intrusion (Fig. 4d, i, k), indicating that they are remnants of the host stratigraphy enclosed by adjacent sills.

## 4. Internal structure of sills

A range of internal textures and fabrics are described below that provide criteria to help distinguish sedimentary sills from depositional beds.

### 4.1. Internal layering

Collinson (1994, p.111) has previously noted that sandstone sills and dykes may show "a marginal foliation parallel with the walls, reflecting shearing during intrusion" (Fig. 1).

In the case study, the internal fabric is sub-parallel to the margins and bridges within the sill, although it locally appears to contain more folding towards the pointed 'bayonet' terminations (Fig. 3d–h). In general, fragments up to 10 cm long may become aligned to create a fabric parallel to the margin of the sill (Fig. 4a–e). In addition, faint laminae are occasionally observed within sills, although homogenous sill matrix with mm-scale aragonite and detrital fragments is more typical (Fig. 5a–f). It is notable that where sills bifurcate and intrude along detachments and faults, the fabric within the injection remains parallel to the margins of the cross-cutting intrusion (Fig. 5g–k).

### 4.2. Grading and brecciation

Angular clasts that form lenses of breccia within sills have been recorded by Archer (1984), while grading of the matrix in sills has been reported by Macdonald and Flecker (2007) (Fig. 1).

In the case study, no grading has been observed within sills, although it is preserved within sedimentary caps that overlie MTDs and were deposited out of suspension following slope failure (Fig. 5a) (e.g. Alsop et al., 2021a; b, 2022). Localized zones of brecciation are developed that comprise disorganised cm-scale angular fragments of laminated host sediment (Fig. 4e, g). Although brecciation is clearly not unique to sills and may form during downslope-directed MTD movement, its presence does not preclude the interpretation of a sill.

## 5. Nature of sill contacts

Most criteria used to recognise sedimentary sills in typically bedded sequences concentrate on the upper margin of the sill, as this is where the nature of intrusive contacts versus conformable depositional boundaries may most clearly be distinguished.

### 5.1. Sharp upper contacts

A number of authors have noted that the upper margins of sills form sharp intrusive contacts that, unlike adjacent depositional beds, lack a gradation into the overlying sediment (e.g. Truswell, 1972; Hiscott, 1979; Archer, 1984).

Within the case study, sills are marked by sharp upper contacts, although this may become more difficult to distinguish where sills are intruded into detrital-rich beds of similar composition to the sill itself (Fig. 4a–d, 5a-d). In addition, the varved nature of lacustrine sediments typically results in widespread sharp contacts, making this criterion potentially less significant in these settings.

### 5.2. Erosive upper contacts

Irregular upper surfaces to sills that erode into the overlying sequence are a defining characteristic, which demonstrate an intrusive origin for sills that cannot be created during deposition of beds (e.g. Macdonald and Flecker, 2007; Hurst et al., 2011) (Fig. 1).

Within the case study, erosive upper contacts are exposed for up to 5 m along individual sills (Fig. 4a–d, 5a-d). Erosion cuts through 10 cm of an established roof stratigraphy above the sill that itself can be correlated for several metres along the upper contact (Fig. 4a–d).

### 5.3. Cross-cutting of laminae in overburden

The erosion and truncation of laminae in host sediments above sills has been reported by a number of authors, including Archer (1984), Kawakami and Kawamura, (2002, p.172) and Palladino et al. (2020, p.5) (Fig. 1). Although such discordant relationships may be difficult to ascertain due to the bed-parallel nature of sills, they are critical pieces of evidence that indicate the overlying strata was already in place at the time of intrusion.

Within the case study, some cross-cutting of overlying stratigraphy is locally observed (e.g. Fig. 3d–f, 4i, j). However, sills are generally bedding-parallel, possibly reflecting the easy planes of intrusion provided by the highly-laminated lacustrine sequence.

### 5.4. Roof pendants

Roof pendants are created where portions of overlying stratigraphy are partially enclosed by the underlying sill, or become entirely detached (e.g. Archer, 1984).

Within the case study, detached parts of the roof sequence, containing a 2 cm thick pale grey-green detrital-rich bed that forms a recognisable stratigraphy, are observed in clasts (Fig. 4g). The correlation of stratigraphy from the detached pendant to the roof confirms the source of the clast to be erosion of the overburden. In most cases,

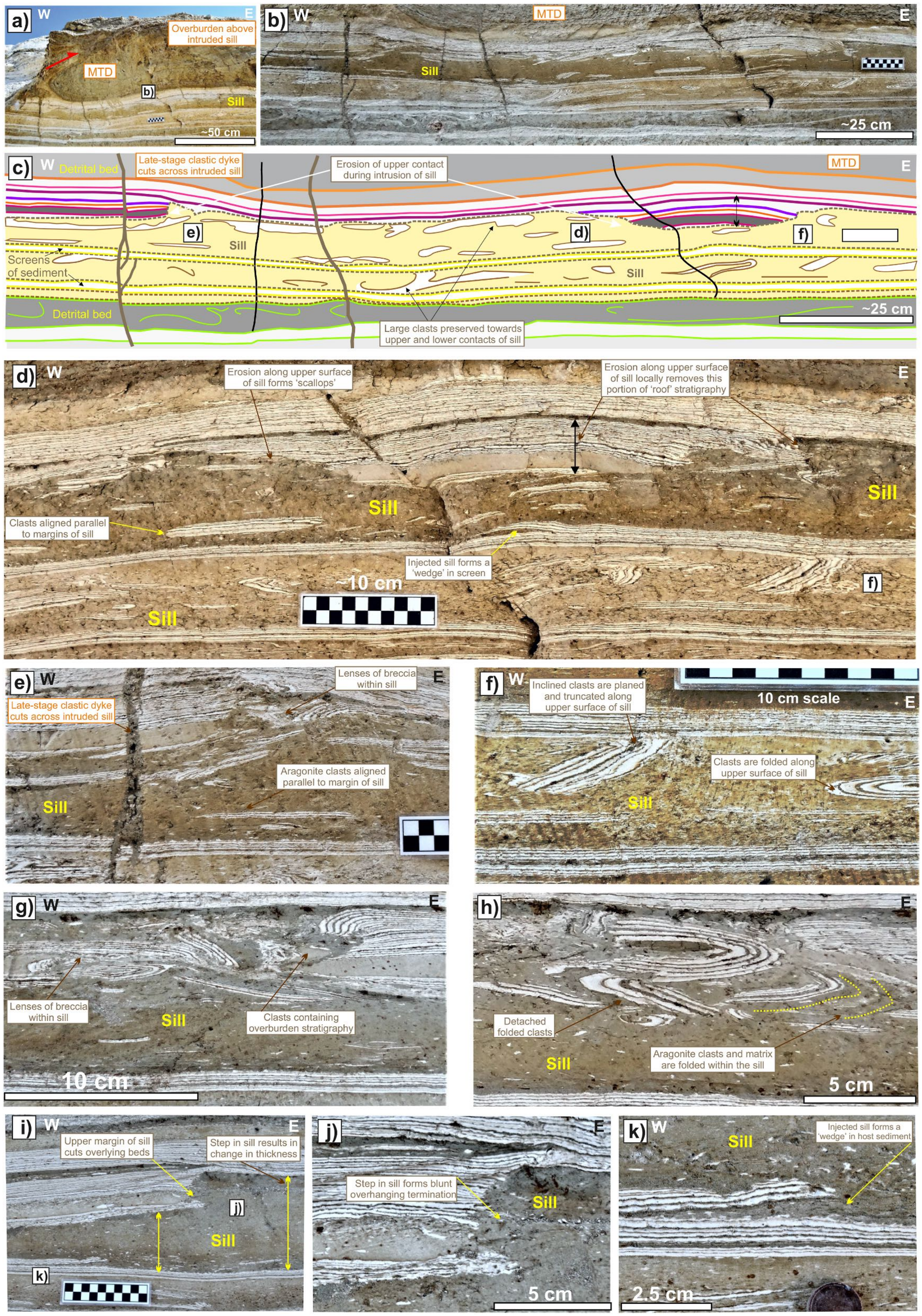


**Fig. 4.** a, b) Mobilization of sediment below an MTD at Peratzim results in a sill intruding into adjacent detrital- and aragonite-rich beds. c) Line drawing highlighting geometry of the sill with an irregular erosive upper contact and containing clasts. Close-up photographs of d) erosive upper contact of sill creating scallops, e) zones of breccia cut by a late-stage clastic dyke, f) truncation of inclined clasts along contacts, g) clasts containing overburden stratigraphy, h) intensely folded clasts and adjacent matrix in the sill, i, j) steps creating changes in the thickness of the sill, and k) injection of the sill into underlying stratigraphy creating wedge geometries (location shown in i). Erosion of overlying laminae can only be achieved after deposition of these younger sediments, thereby demonstrating that intrusion of the sill took place below the immediate sediment surface.

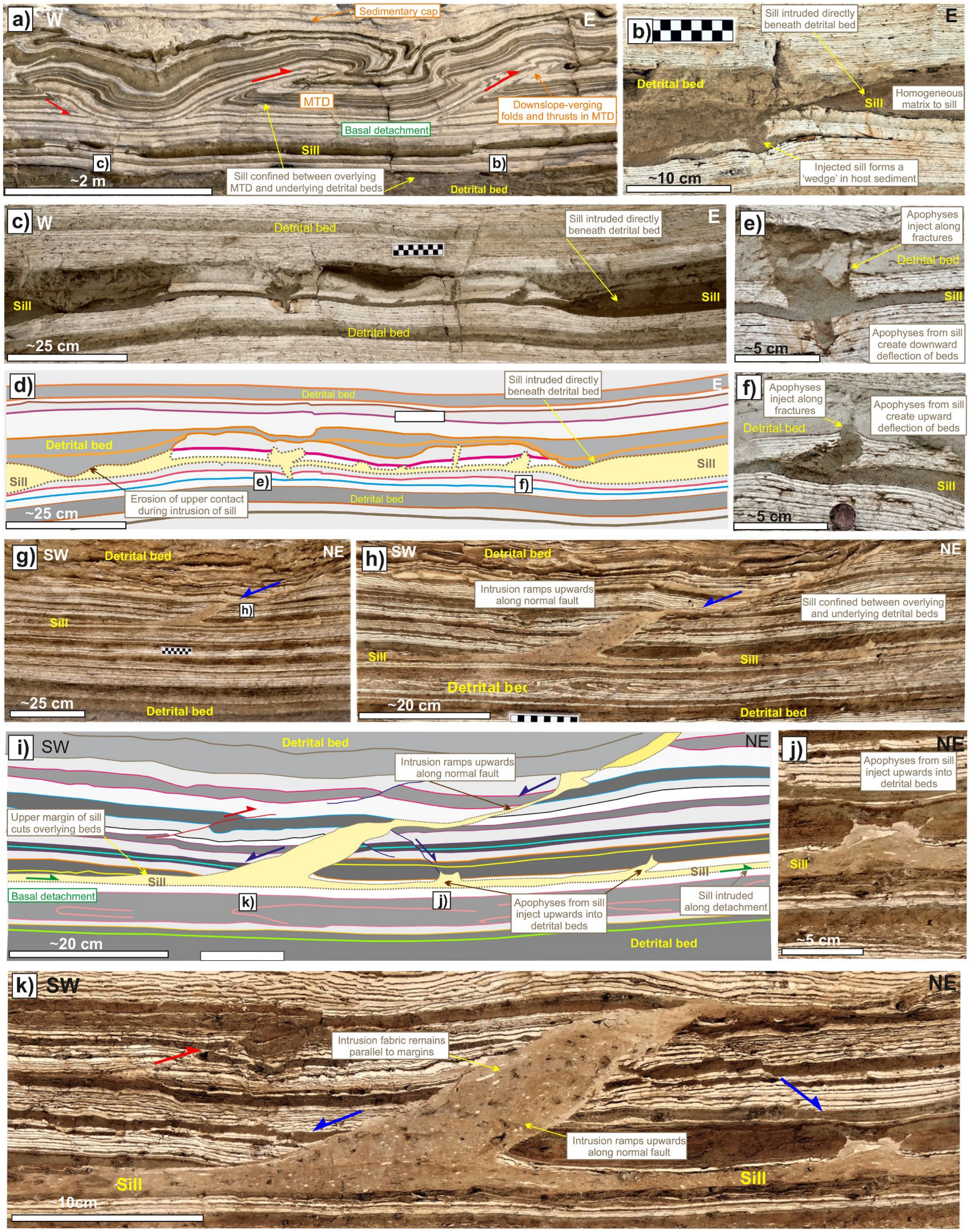


**Fig. 5.** a) Photograph of folds and thrusts in an MTD with an overlying sedimentary cap and an underlying sedimentary sill (Peratzim). b) Details of the sill (see (a) for position) showing sediment injection into the underlying laminae. c) Photograph and d) line drawing of the sill intruded beneath a detrital bed with local apophyses that inject e) downwards and f) upwards into adjacent stratigraphy. g) Overview photograph, h) photograph, and i) line drawing of bed-parallel sill and sediment intrusion along a normal fault (Miflat). Details of apophyses (j) and intrusion-parallel fabric (k) indicate injection of sediment.

however, the clasts are fragmented and disaggregated to such an extent that no stratigraphy is discernible.

### 5.5. Apophyses emanating from sills

The presence of sills in an otherwise bedded sequence may be detected by small offshoots emanating from the sill (e.g. Truswell, 1972; Hiscott, 1979) (Fig. 1).

Within the case study, cm-scale apophyses of sills inject both upwards and downwards into the adjacent stratigraphy (Fig. 5a–f). The margins of apophyses are sharp and associated with fractures that terminate in more competent detrital beds in the stratigraphy (Fig. 5e and f). Where apophyses inject above the sill, then they deflect the overlying stratigraphy upwards, whereas injection beneath the sill leads to downwards deflections (Fig. 5e and f). In each case, the stratigraphy on either side of the apophyses is not offset across fractures, but simply deflected by the intrusion.

## 6. Clasts preserved within sills

Fragments of adjacent stratigraphy form intra-clasts (or more simply clasts) preserved within sills. Although clasts may be incorporated into a variety of sedimentary deposits across a broad range of environments, their distribution, geometry and detailed cross-cutting relationships aid in the identification of sills.

### *6.1. Distribution of large clasts*

A number of authors have noted that clasts may be concentrated towards both the upper and lower contacts of sedimentary sills (e.g. Truswell, 1972; Kawakami and Kawamura, 2002; Macdonald and Flecker, 2007; Hurst et al., 2011; Palladino et al., 2020).

Within the case study, larger clasts of laminated aragonite up to 20 cm in length are preserved towards both the upper and lower contacts of sills (e.g. Fig. 4a–h). There is no discernible grading of these clasts next to the margins of the sill.

### *6.2. Clasts cut by upper surface of sill*

Kawakami and Kawamura (2002) observed 'flatly planed clasts' within a sill that were abruptly truncated by the upper intrusive contact.

Within the case study, truncation of clasts is best observed where the clasts are inclined and the horizontal contact of the sill cuts directly across the laminae in the clast (Fig. 4d, f). Laminae in the excised clasts display folding and deformation immediately adjacent to the sill contact. The laminae in the host sediment immediately above the truncated clast show no depositional variation in thickness or composition, indicating that clasts had not influenced sedimentation, thereby supporting the intrusive sub-surface origin of the sill (Fig. 4d, f).

### *6.3. Alignment of clasts*

Previous authors have reported that clasts are frequently aligned parallel to the margins of sills (e.g. Archer, 1984; Kawakami and Kawamura, 2002; Hurst et al., 2011, p.221).

Within the case study, aragonite laminae form highly-elongated clasts up to 20 cm in length that are generally parallel to the margins of the sill, and to sediment screens within sills (e.g. Fig. 4d).

### *6.4. Clasts contain overlying stratigraphy*

Within the case study, some clasts contain portions of stratigraphy that can be correlated with that in the overlying sequence above the sill (Fig. 4g). In this situation, such clasts can only have been derived from the overlying stratigraphy, indicating that an intrusive sill contact cuts the finer-grained detrital layer in the overlying sequence.

### *6.5. Folded clasts*

Previous authors have noted that clasts within sills may be tightly and recumbently folded, or even imbricated (e.g. Kawakami and Kawamura, 2002, p.175).

Within the case study, such folded clasts are frequently observed (e.g. Fig. 4f–h) despite the underlying and overlying aragonite laminae adjacent to the sill showing no evidence of folding. No imbrication of clasts has been observed in the present study.

## 7. Folding and deformation on margins of sills

Intrusion of sedimentary sills creates a variety of features associated with deformation and folding of the host sediment that may be used to distinguish sills from depositional units.

### *7.1. Bed-parallel wedging*

Sedimentary sills may locally intrude and create 'wedge-shaped' fissures parallel to the lamination in the host sediment (e.g. Kawakami and Kawamura, 2002).

Within the case study, m-scale wedges may form at the termination of sills to create 'pointed bayonet' geometries (e.g. Fig. 3d–h), or at a cm-scale where wedges of injected sediment develop on the upper or lower contacts of the sill, highlighting its intrusive character (Figs. 4k and 5a, b). Wedging of intrusive sills is generally developed along particular beds and is parallel to laminae, thereby providing an insight into the strong control exerted by layering on the intrusive process (Figs. 4k and 5b).

### *7.2. Folding on margins of sills*

Within the case study, host strata that elsewhere is undeformed may locally be intensely folded along the margins of sills. Such folds, which are generally recumbent and tight-isoclinal, are developed above wedges of intrusive sediment, indicating that the localized folding was created during injection of the sill rather than being related to MTDs (Fig. 6a–h, 7a-f).

In our first example, the upper margin of the sill cuts across laminae in the overlying sequence while the lower contact remains bed-parallel or forms wedges that intrude into the underlying beds (Fig. 6a–c). A small vertical sediment intrusion injects upwards from the sill and cuts overlying beds that are locally deflected (Fig. 6a–c). The deflected beds, together with the intrusion, are truncated by overlying stratigraphy, indicating a possible unconformity or detachment surface (Fig. 6a–c, f). Along the lower margin of the sill, an isoclinal fold with an overturned upper limb is formed in host aragonite-detrital laminated sediments (Fig. 6a–c). Dip isogon analysis (Ramsay, 1967) shows that the aragonite-rich units form a fold with slightly thinned limbs compared to the hinge (Class 1C), whereas the detrital-rich beds maintain thickness on the lower limb (Class 1B) and hinge and are only slightly thinned on the overturned limb (Class 1C) (Fig. 6b, d). Greater thinning of aragonite- and detrital-rich layers on the upper limb of the fold reflects overturning of these beds.

The upper limb terminates in a downward deflecting tip that creates a 'barb' in the overall 'fish hook' shaped fold (Fig. 6c, e). The sill occupies the fold core and also penetrates into the stratigraphy underlying the folded horizon (Fig. 6a, e). Within the sill, a fabric defined by elongate mm-scale aragonite and detrital fragments is generally parallel to the margins of the sill. Adjacent to the isoclinal fold closure, it is wrapped around the hinge suggesting it has also been folded (Fig. 6b). The outer arc of the fold hinge is defined by a detrital layer and is associated with extensional fracturing along which minor intrusions of sill are injected (Fig. 6b). The preserved length of the overturned fold limb (~80 cm) is considerably longer than the thickness of the sill at this site (~20 cm) (Fig. 6c). A smaller recumbent fold with sheared upper limb is preserved immediately to the E (Fig. 6c, f, g), suggesting that the folding process may have been repeated along the base of the sill.

In our second example, the upper and lower contacts of the sill are parallel to bedding, but locally create wedge-shaped terminations that intrude into the host stratigraphy (Fig. 7a and b). Segments of the sill are intruded above and below marker stratigraphy, which creates bridges that separate the lateral terminations of each segment (Fig. 7a–d). Stratigraphy is locally 'jacked-up' adjacent to the sill, with stratigraphic contacts being preserved at the upper tips of the injected sill segment (Fig. 7d and e). In some cases, the lateral terminations of segments form

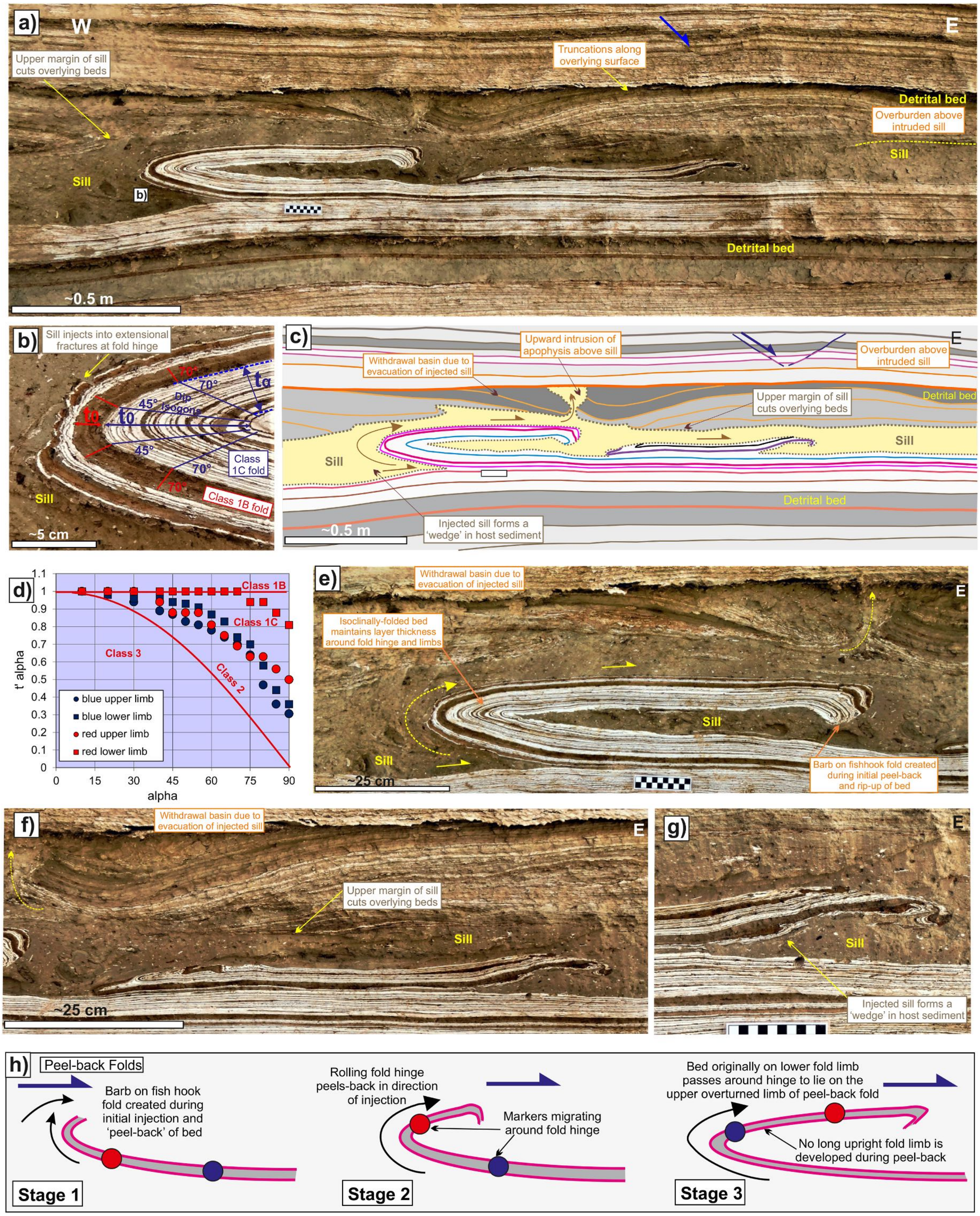


**Fig. 6.** a) Photograph, b) detail of fold hinge, and c) associated line drawing of 'peel-back' folds developed in a sill (Miflat). In b) dip isogons are drawn at representative angles (α) of 70° and 45° across aragonite (blue) and detrital (red) beds around the hinge of the fold. The thickness of beds along the axial surface ($t_0$) is compared with the orthogonal thickness ($t_\alpha$). d) t'alpha graph (where $t'_\alpha = t_\alpha/t_0$) plotted against dip angle (α) to create a series of fold classes from data shown in b) (Ramsay 1967, p.366). The sill truncates overlying beds, and in e) shows evidence of upward expulsion of sediment (see also c). f) Detail of truncation of overlying layers, and g) injection of sill beneath host sediment to create a wedge. h) Schematic cartoon illustrating the three stages in the evolution of a peel-back fold. In stage 1 (left), intrusion of the sill creates a marked fold or 'barb' in host sediment as sediment is injected beneath and jacks-up underlying beds. In stage 2, continued intrusion causes a rolling fold hinge with the deformed bed peeling back in the direction of sill injection. In stage 3 (right), markers originally on the lower limb of the fold have rolled around the fold hinge to lie on the upper limb. The peel-back mechanism does not require a long upright limb to pass around the fold hinge and may therefore develop in relatively thin sills. The rolling fold hinge results in tight-isoclinal folds where competent (detrital) layers broadly maintain bed thickness. (For interpretation of the references to colour in this figure legend, the reader is referred to the Web version of this article.)

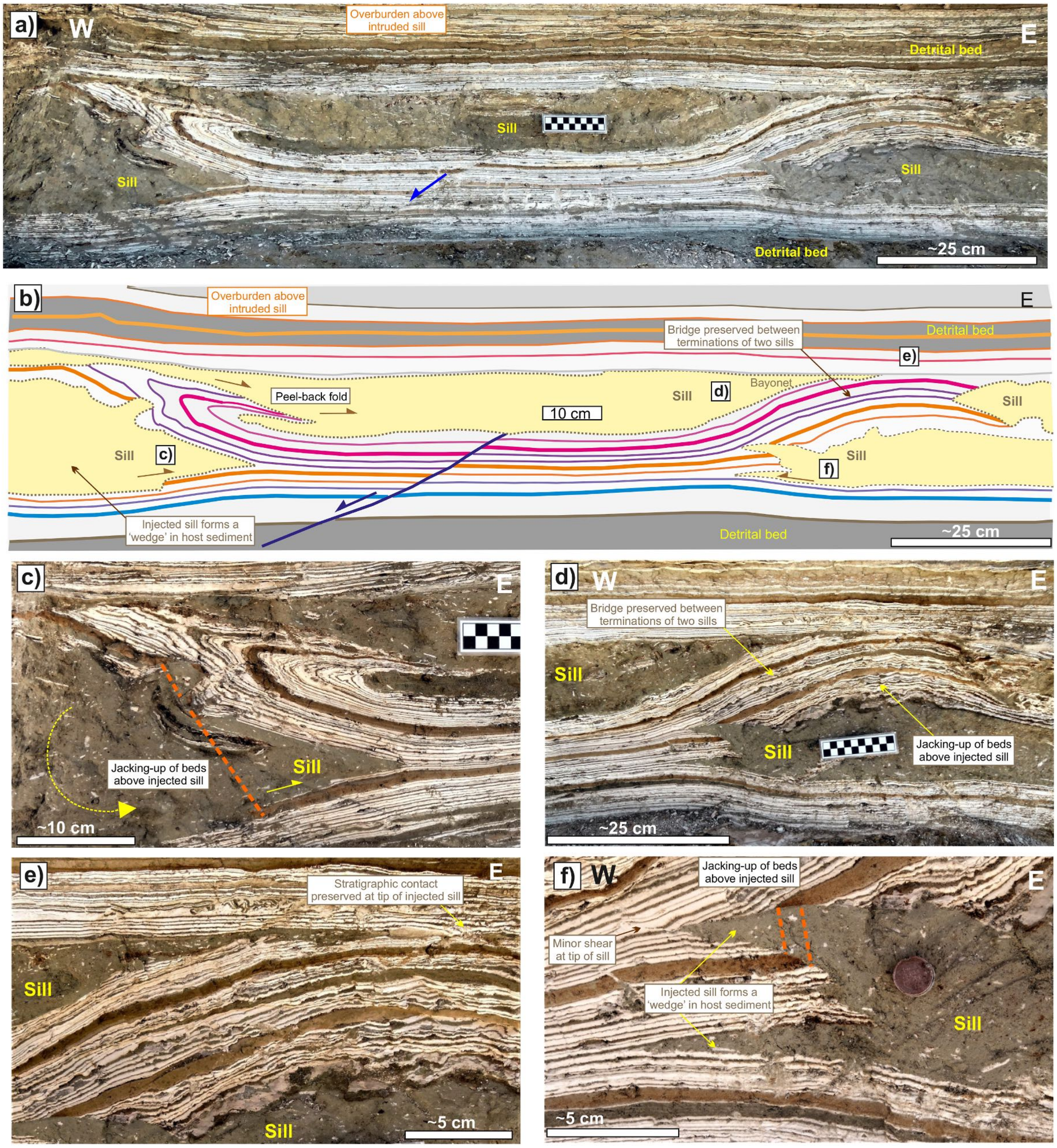


**Fig. 7.** a) Photograph and b) associated line drawing of 'peel-back' folds and sediment bridge developed in a sill (Miflat). c) Photograph of 'jacking-up' of beds above a sill that forms a wedge. d) Photograph of sediment bridge with overlying sill segment (left) terminating in a pointed bayonet, while the lower sill (right) forms a double-pronged termination. Details of the upper stratigraphic contact of the bridge are shown in e), while photograph f) shows a close-up of sill terminations and associated fracturing.

two fingers that inject parallel to bedding, or cross-cut more competent (detrital) beds where the tips of the intrusion are marked by minor shears (Fig. 7f). Intrusion of the sill creates isoclinal folds, with the upper limb of the fold being overturned and sheared out, while the fold core is occupied by the sill (Fig. 7a–f). In both of our examples, the upper fold limbs are overturned towards the east, although we have also observed overturning towards the west. The propagation direction of sill intrusion may be perpendicular to the viewer and 'out of plane', if structures in igneous sills are used as an analogy (e.g. Baer, 1993).

## 8. Sills associated with downslope-directed thrusting and folding

Intrastratal detachments form within the sub-surface and result in overburden sliding downslope towards the east or northeast and the depocentre of the basin. Detachments are typically parallel to bedding, although may locally transect and offset earlier faults and thereby provide an estimate of displacement (Alsop et al., 2020a). Sediment injections are formed of remobilised sediment that comprises a fine-grained aragonite and detrital mixture containing larger cm-scale clasts of laminated sediment. Some of this injected sediment was previously described as gouge by Alsop et al. (2018), although it clearly may intrude upwards from detachments at the base of FATS and MTDs.

### 8.1. Intrusion of sills along basal detachments to folds

Sills in the case study form along basal detachments, which translate overlying strata downslope, resulting in recumbent or upright folds that are detached directly on the sill (Fig. 8a–f). The overturned limbs of downslope-verging recumbent folds are sharply truncated by sills (Fig. 8a–f). More upright anticlines that also 'ride' on detachments marked by sills are associated with sedimentary dykes that intrude upwards, and potentially out of plane, from detrital-rich beds in the cores of anticlines, suggesting high fluid pressures (Fig. 8e and f). The 'pinched' shape of the folded detrital layer implies a 'hinge-collapse' scenario (e.g. Fossen, 2016, p.273), with the detrital-rich layer feeding the intrusions (Fig. 8e and f). Sediment injections extending above the deformed horizon indicates that intrusions either develop after the MTD had formed, or the folds were created in the shallow sub-surface during intrastratal deformation (Fig. 8a–f, 9a-d). Folds detaching on underlying sills, together with the intense sheared fabric within the sills (Fig. 8c and d) suggests that intrusions are syn-deformational with high fluid pressures facilitating downslope movement of sediment.

### 8.2. Intrusion of sills along basal detachments and thrust ramps

Downslope-verging FATS detach on underlying sills that are <10 cm thick and locally cut across fold hinges (Fig. 8g–i). The underlying stratigraphy remains unfolded and parallel to the intrusions, which contain elongate aragonite fragments aligned parallel to the contacts (Fig. 8g–i). The sediment injection with marked internal fabric forms a basal detachment or 'floor thrust' to the system. Sediment injections also form along thrust ramps, with localised 'fingers' intruding upwards and cross-cutting the folds overlying the ramp (Fig. 9a–d). Detrital layers form buckle folds suggesting that they were relatively competent at the time of deformation and were then cross-cut by intrusions. In. Fig. 9e–k, the fingers of homogenous detrital-rich sill have intruded along particular horizons of aragonite-rich host sediment. Adjacent sills may locally join one another via linking dykes that cross-cut stratigraphy. In some cases, sills display 'frilled' margins where the intrusive contact is irregular on the scale of mm-cm (Fig. 9g). Injections may be cut by thrusts that also affect the overlying sequence, indicating that sills were intruded into the sub-surface prior to gravity-driven deformation.

### 8.3. Intrusions of sills along roof detachments to FATS

Where roof detachments are developed above FATS, deformation is considered to form beneath a sedimentary overburden in the sub-surface (Alsop et al., 2021a, b). Sills are intruded above FATS in positions where roof detachments generally form, thereby masking any such detachments (Fig. 10a–g). The lack of a sedimentary cap, coupled with the style of buckle folding of detrital units, indicates competent beds, and is consistent with sub-surface folding and thrusting (Fig. 10a–g). The sill varies in thickness from 3 cm to 10 cm and contains aligned aragonite and detrital fragments that parallel the margins of the sill (Fig. 10c–g). The upper surface of the sill is irregular and cuts across the overlying sequence, while the lower contact truncates underlying folds and thrusts that verge towards the E (Fig. 10a–g). The truncation of underlying folds, coupled with the sill being deformed by underlying thrusts, is consistent with intrusion during downslope-directed sub-surface deformation.

## 9. Sills associated with downslope-directed extension and normal faulting

### 9.1. Sediment injection along normal faults

Sediment injections in the case study can intrude directly along normal faults that cut across stratigraphy (Fig. 5g–k). In these examples, the normal faults are assumed to have rooted into underlying detachments that are now masked by the sill (Fig. 5g–k). Small elongate 'flakes' of aragonite within the injections are parallel to the margins of the intrusion along detachments and normal faults, indicating that the intrusion was a single event rather than multiple episodes. Development of injected sediment along both detachments and normal faults suggests that they potentially operated at the same time.

### 9.2. Sills along detachments

Sills up to 5 cm thick may form directly along bedding-parallel detachments (Fig. 11a–d). Overlying normal faults become listric and flatten into the injection marking the detachment, while the upper parts of the normal faults are also cut by a detachment. Truncation of marker beds (shown in purple) by the sill is consistent with extensional movement. In Fig. 11e–h, the sill forms a wedge beneath a rotated package of overlying strata that resembles a listric fault. Fingers of the sill locally intrude above the rotated sediment, while the top of the sill gently transects across the overlying stratigraphy that forms a 'roll-over' anticline (Fig. 11 e-h). Injection of the sill both beneath the listric fault, and locally above rotated beds, suggests that it was intruded during the extensional movement. Downslope-dipping normal faults are marked by breccia zones up to 10 cm wide that are offset by later normal faults and underlying sediment sills along detachments (Fig. 11i–k). Normal faults may either sole into the underlying detachment and sedimentary injection or cut across it. The steep breccia zones may be created by tension formed during downslope slip above the detachment and injections (Fig. 11 l, m). The injection of sills along detachments is consistent with intrusion during extension associated with downslope movement of sediments.

### 9.3. Sills cut by normal faults

Sedimentary sills may display a range of timing relationships (from 1 being the oldest to 3 being the youngest) relative to adjacent normal faults created during downslope movement of sediments. In the simplest scenario, bedding-parallel sills are cut and offset by normal faults (Fig. 12a–c). The normal faults are later displaced by bed-parallel slip (BPS) formed along detachments to create sawtooth or staircase geometries (Fig. 12a–c) (see Alsop et al., 2020a for terminology). These relationships suggest that the sills largely pre-date the later faulting and detachments. In another situation, sills are cut by normal faults (1), with these faults later offset by BPS detachments (2) (Fig. 12d–g). Detachments are cut by subsequent normal faults (3), while sills are locally remobilised to cut the early normal faults (1) (Fig. 12d–g). In a similar example, sediment injections form along an early BPS detachment (1), that is subsequently offset by normal faults (2), (Fig. 12h and i). The early detachments are later reactivated (3) resulting in remobilization of sediment and minor offset of normal faults (2) (Fig. 12h and i). Although sills and sediment injections are locally cut by normal faults, the subsequent offset of normal faults by BPS along detachments, that may also develop sills, collectively indicates that the timing of sills, BPS detachments and normal faults are intimately related and broadly contemporaneous with one another.

## 10. AMS analysis of injected sediment sills

Although AMS has seldom been used in the analysis of sills within the Lisan Formation (but see Levi et al., 2006b, their Fig. 8 [B1]), it has been employed in the analysis of injection directions in clastic dykes (Levi et al., 2006a, b; Jacoby et al., 2015). In MTDs and slumps of lacustrine sediments, $K_1$ axes become aligned with the orientation of fold hinges, and $K_3$ axes parallel to the poles of associated axial planes, showing a trail of orientations directed towards the absolute transport direction at the depocentre of the basin (Weinberger et al., 2017, 2022; Alsop et al., 2020b) (see section 1.2). The aragonite and the detritus layers of the Lisan Formation are diamagnetic and paramagnetic, respectively, while the bulk magnetic susceptibility is typically positive. Titanomagnetite, magnetite, and greigite are the ferromagnetic carriers in the detrital laminae (e.g. Ron et al., 2006; Levi et al., 2006a, 2014).

In this case study we analysed the magnetic fabrics of 9 samples from

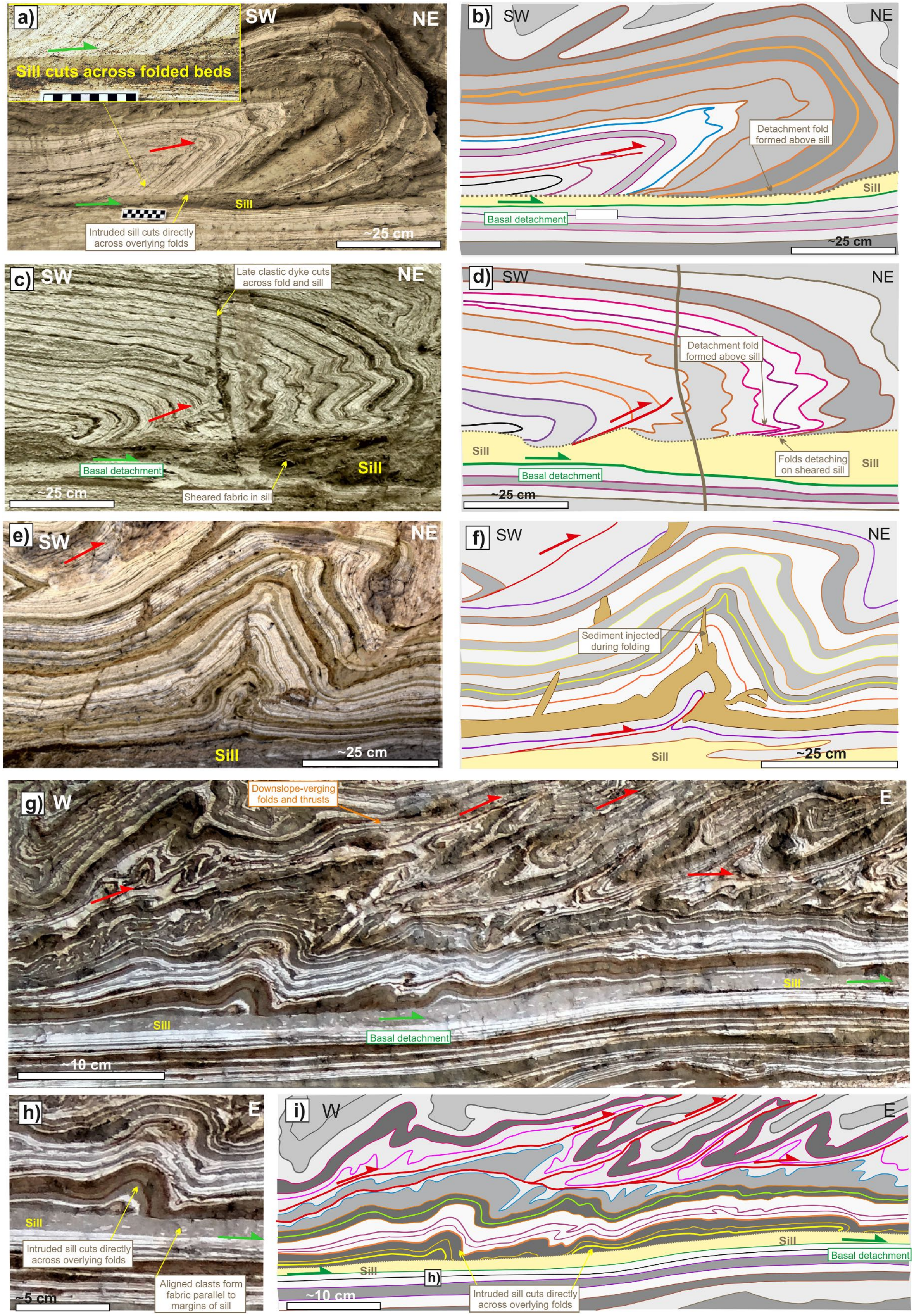


**Fig. 8.** a, c, e) Photographs and b, d, f) associated line drawings of downslope-verging folds formed directly above sills that intrude along the basal detachments (Peratzim). Overlying folded beds appear to detach on the sheared sills. g) Sill developed along a basal detachment with h) detail of a fold truncated by the sill and i) overall line drawing (Miflat). Truncation of folds associated with the fold and thrust system indicates that the sill was intruded along the basal detachment during deformation.

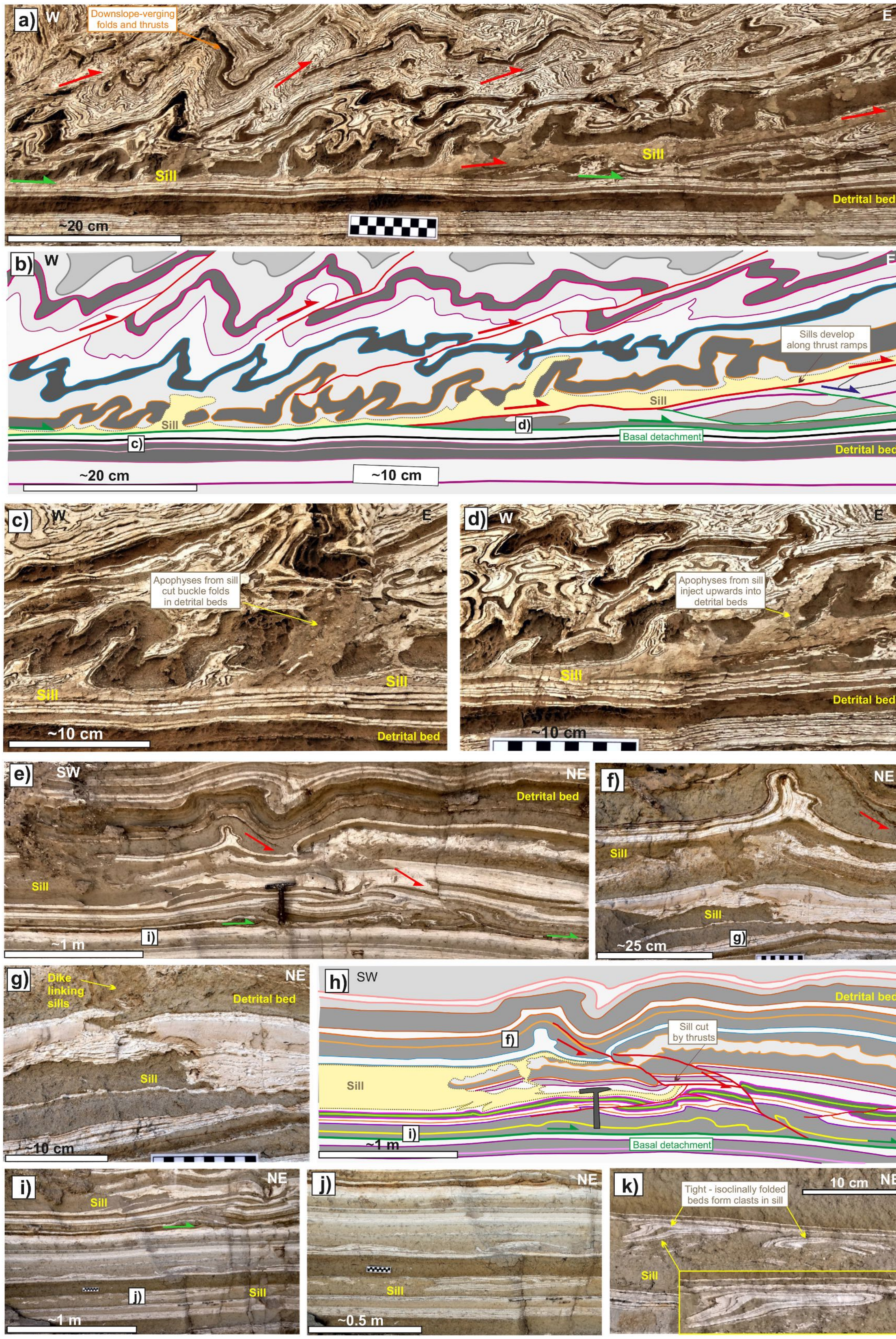


**Fig. 9.** a) Photograph and b) line drawing of sill formed along a bed-parallel detachment and thrust ramp that cuts overlying stratigraphy. c) Apophyses from bed-parallel sill, and d) sill along thrust ramp cut overlying buckle folds in detrital beds (see (b) for positions). This suggests a component of shortening and buckling prior to intrusion of apophyses. e) Sill intruded in the footwall of a backthrust with f, g) showing details of local cross-cutting relationships. h) Line drawing highlighting position of sill beneath a backthrust with local cut-offs by thrusts, suggesting that the sill was intruded during contraction. i) Photograph and j) close-up of sills intruded beneath the basal detachment to the thrust system, with sills containing k) isoclinally folded clasts.

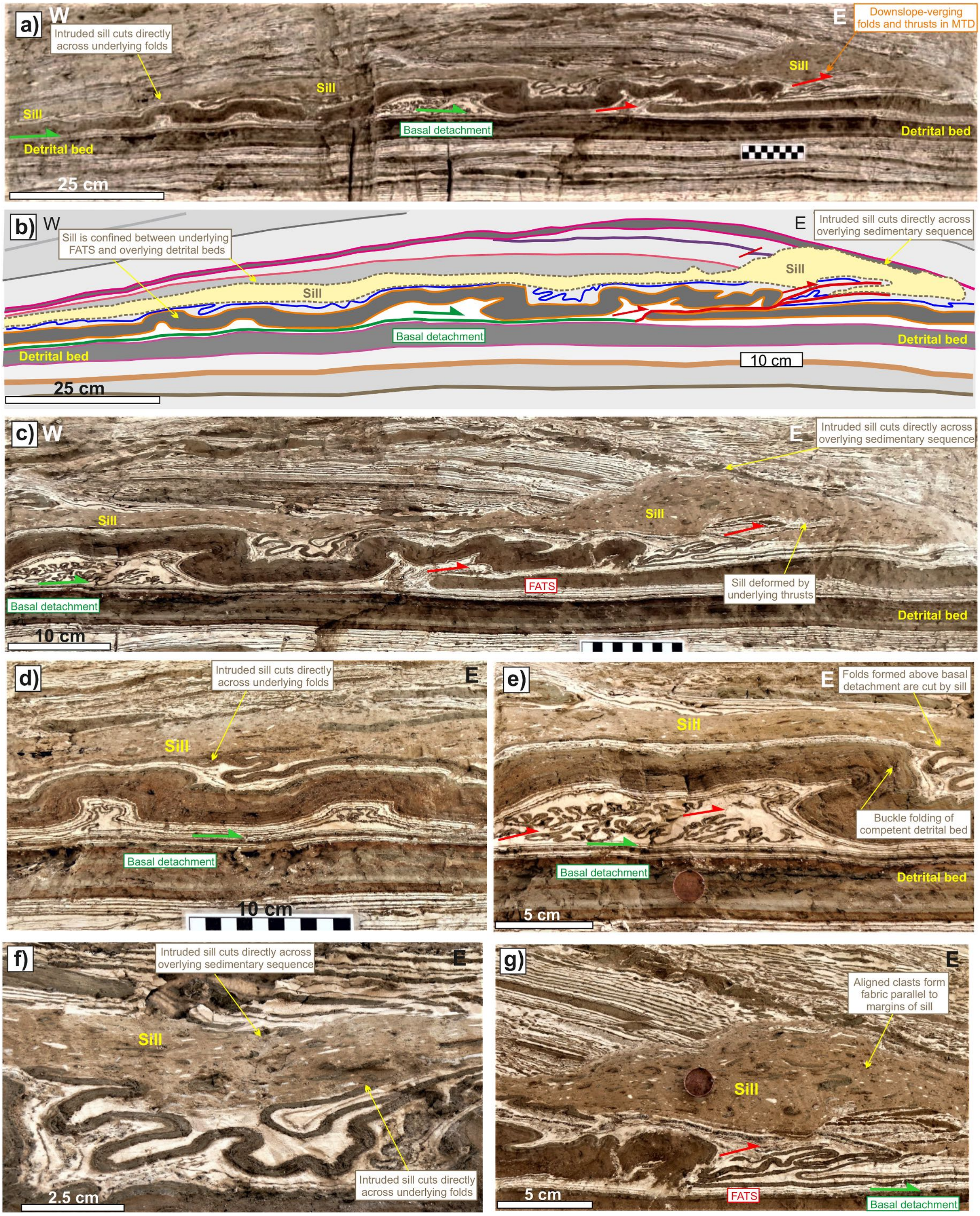


**Fig. 10.** a) Photograph and b) associated line drawing showing a fold and thrust system (FATS) that is overlain by an intruded sill (Miflat). The FATS does not display a sedimentary cap and is considered to form in the sub-surface. c) Sedimentary sill cross-cuts overlying inclined beds and folds, but is locally affected by thrusts ramping from the basal detachment, indicating it was intruded during deformation. d, e) Details of folding of the competent detrital bed above the basal detachment and the cross-cutting relationships of the sill. f, g) Close-up photographs showing an alignment of clasts and fabric within the sill and cross cutting of underlying folds linked to FATS.

a sill exposed at Peratzim (Fig. 13a). The magnetic fabrics developed in this sill (Fig. 4a–c, 13a) are strongly oblate with clustered $K_1$ and $K_2$ axes being clearly distinguishable, while $K_3$ axes are off vertical (Fig. 13b and c). Based on the orientation trails of these $K_3$ axes, the weak deformation magnetic fabric suggests horizontal flow within the sill that is directed towards the SE (see details of technique in Levi et al., 2006b; Weinberger et al., 2017). Intrusion and flow in the sill towards the SE are parallel to the strike of the overlying fold and thrust structures within the MTDs.

## 11. Discussion

### 11.1. What controls the location of sills?

The intrusion of sills is created by high fluid pressures that fluidize

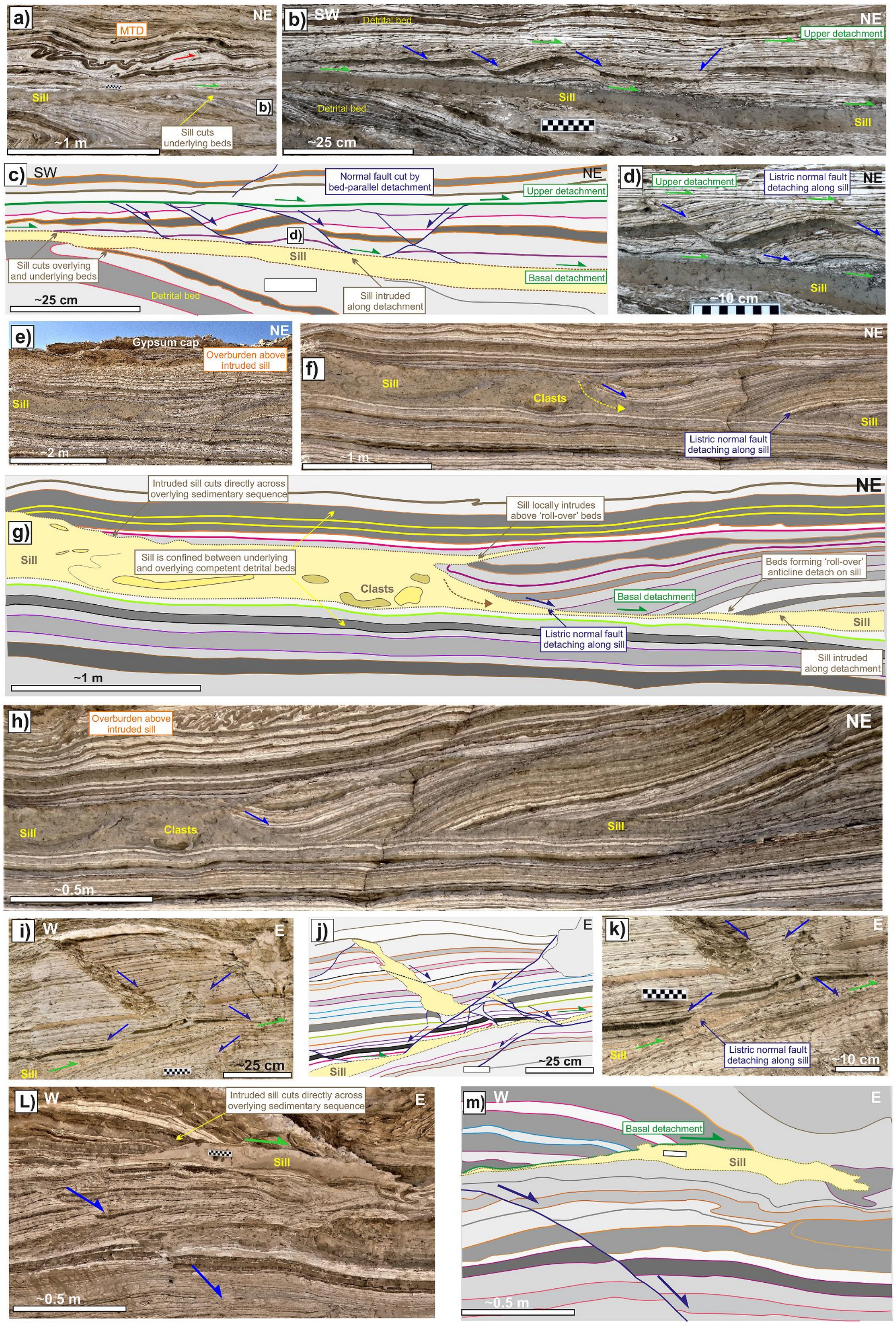


**Fig. 11.** a) General view and b) photograph with c) associated line drawing of normal faults developed between an upper detachment and basal detachment marked by a sill. d) Close-up photograph of listric normal faults rotating into the basal detachment directly above the sill, suggesting the sill was emplaced during extension. e) General view and f) photograph with g) associated line drawing of a listric normal fault being intruded by a sill. The sill cuts across overlying stratigraphy (SW side of photo) and also forms a pointed bayonet termination above the listric fault. h) Close-up photograph showing intrusion of the sill along the basal detachment to the listric normal fault, suggesting the sill was emplaced during extension. Note the preservation of clasts within the sill. i) Photograph and j) associated line drawing of conjugate normal faults detaching on an underlying sill. The east-dipping normal fault is marked by breccia and mobilised sediment. k) Close-up photograph showing details of the normal faults detaching on the underlying sill, suggesting it was emplaced during extension. L) Photograph and m) associated line drawing of a sill and detachment cutting across overlying stratigraphy that is inclined towards the east. The sill is considered to be emplaced during extension associated with the basal detachment.

sediment leading to its injection within bedded sequences. Increases in fluid pressure may be generated by a variety of factors including glacial loading (e.g. Phillips et al., 2013), sediment overloading and storm waves, although earthquakes are also frequently cited and are considered the likely source in the Lisan Formation (Levi et al., 2006b, 2008, 2011) and this study. Indeed, Hiscott (1979, p.6) notes that "earthquakes may have been responsible for both slumping and liquefaction". Increases in fluid pressure are locally controlled by baffles or barriers to fluid flow that, in the present study, include thick detrital beds, deformed FATS and MTD horizons, or gypsum units (Fig. 11e). The importance of overlying seals that allow fluid pressure to build up within a sequence prior to the intrusion of sedimentary sills has been recognised by Hiscott (1979) (see also Ogata et al., 2014a).

We have presented a number of examples in this case study of sills being bound above and below by thicker detrital-rich horizons that presumably trapped fluids and encouraged mobilization and injection of sediment during seismic events (Fig. 4a–d, 5a-f). The recognition of bed-parallel sills adjacent to such detrital horizons may, however, be problematic, as sills are composed of mixed aragonite and detrital sediment that superficially resembles the detrital beds (Fig. 5a–f).

FATS may detach on sills suggesting that intrusion of the sediment occurred during downslope shearing (Figs. 8, 9a-d). The development of sills above FATS in a position occupied by a roof detachment (Fig. 10) indicates that deformation occurred in the sub-surface (Alsop et al., 2022). In such situations, extreme care needs to be taken that sills are not confused with the mixed aragonite-detrital capping layers that are deposited out of suspension following surficial failure of MTDs (e.g. Alsop et al., 2021a, b). The inability to distinguish injected sills from sedimentary caps in buried sequences may lead to the misidentification of sub-surface FATS and surficial MTDs.

Sills can form parallel to the basal shear zone of MTDs, which may be more competent than the host stratigraphy due to de-watering and seismic strengthening (Fig. 4a–d, 5a-f). Sills also intrude above slumps (e.g. Hiscott, 1979, p.6), although they generally form beneath MTDs that were created at the sediment surface and subsequently acted as local baffles to fluid migration. In some cases, sills with erosive upper contacts lie just 10 cm below the base of the overlying MTD (Fig. 4a–d). Hiscott (1979, p.6) notes that "subsequent slumps, however, may have loaded pre-existing deposits, causing liquefaction and mobilization of sands". The suggestion is that mobilization and intrusion of the sill may have taken place during this subsequent slump event. It is possible that fluid pressures are increased by thickening associated with thrusting and folding within the overlying slump, which ultimately leads to injection of the sill. Similar intrastratal deformation triggered by emplacement of overlying MTDs has been previously suggested (e.g. Auchter et al., 2016).

However, slumps and MTDs within the Lisan Formation are generally relatively thin (frequently $<1$ m) and would therefore result in only a limited increase in fluid pressure associated with loading. For example, we calculate that if the sediment was under a 50 m water column and below 2 m of sediment overburden, the estimated pressure was around 0.66 MPa. An extra 1 m of sediment emplaced during MTD movement is about 0.02 MPa (i.e. at least an order of magnitude less than the vertical pressure). Such a small addition of pressure may not be significant enough to cause fluidization, and it is therefore possible that other potential mechanisms, including pressure build-up during the passage of seismic P waves, may lead to fluidization and injection of sills. It is generally considered that earthquakes with $M > 5$ represents the minimum magnitude capable of temporarily transforming sediments from grain-supported to fluid-supported, leading to deformation and injection of sills and dykes (e.g. Leeder, 1987; Ambraseys, 1988; Leila et al., 2022).

### 11.2. Is deformation associated with intrusion of sills?

Intrusion of igneous sills into shallow unconsolidated sequences can lead to soft-sediment folding and thrusting in the adjacent host sediments (e.g. Duffield et al., 1986). Thrusting and folding of sediments may form at the tips of propagating igneous sills and magma fingers (e.g. Schofield et al., 2012; Spacapan et al., 2017) and is considered part of the intrusive process. Although Duranti and Hurst (2004, p.18) have noted from studies of drill cores that deformation frequently develops in beds adjacent to sedimentary sills, there is a general lack of detailed reports of such deformation. We now discuss the folding mechanisms developed along the margins of sills in the case study.

#### 11.2.1. How are peel-back folds created along the margins of sills?

An intriguing question arises from this case study as to how recumbent isoclinal folds with overturned limbs longer than the thickness of the intruded sill are created (e.g. Fig. 6). Clearly, the entire overturned limb cannot have rotated as a single entity through the vertical in a 'fixed hinge' fold model as the thickness of the sill is too thin to allow this.

Flume experiments have previously been used to examine shear-derived folding and mixing between granular flows and underlying loose substrates (Rowley et al., 2011). Given that mobilization of sediment to create sills involves liquidization, we suggest that the experiments of Rowley et al. (2011) on granular flows are also applicable to sedimentary sills. Rowley et al. (2011, their Fig. 5) created recumbent tight-isoclinal folds within the substrate that locally refold and wrap-around the granular flow material. Rowley et al. (2011, p.876) note a number of key points that are consistent with the peel-back folds of the present study: 1) continuous stratigraphy is preserved around the recumbent fold; 2) wrapping of flow material within the core of the fold demonstrates that the folding was created at the base of the flow rather than at the tip of the flow; 3) the distal (down-shear) termination of the fold is "deflected or smeared out"; 4) inverted stratigraphy is created around the fold, "as shear results in rotation during its development"; and 5) more than one recumbent fold may develop beneath flows with a potential for periodicity in structures. We suggest that the granular flow structures described by Rowley et al. (2011) are similar to features produced during rapid injection of liquidized sedimentary sills into water-rich shallow sediments.

In this case study, we interpret folds created along the margins of sills to be formed by a peel-back mechanism whereby shear exerted by the injection of the sill locally rips up and peels back beds of the host sediment (Fig. 6h). The rolling hinge migrates in the direction of shear with 'markers' on the lower limb still attached to the substrate passing around the hinge onto the overturned upper limb (Fig. 6h). This peel-back fold mechanism directly accounts for the following observations:

i) *Length of fold limbs* – The migrating hinge, where any point on the bed passes from the lower limb, around the hinge and onto the upper limb, does not require a thick sill because the length of the entire upper limb (80 cm) did not pass through the vertical at any single point (Fig. 6h). The limb simply rolled around the hinge as it peeled back in the direction of intrusion. This mechanism, akin to rolling-back the lid of a sardine tin, is therefore capable of creating isoclinal folds with long overturned limbs in relatively thin sills (Fig. 6h).
ii) *Thickness of fold limbs* – The overturned limb of the peel-back fold is slightly thinned compared to the lower limb to create Class 1B and 1C folds (Fig. 6b, d). However, despite the recumbent and isoclinal nature of this fold, it does not attain a Class 2 geometry as observed in recumbent isoclinal folds developed within MTDs (see Alsop et al., 2020c, their Fig. 6). While it could be argued that differing fold geometries next to sills simply reflect non-profile views of folds, it should be noted that vertical cliff sections oblique to the exact profile plane of the horizontal fold hinge will only exaggerate the thickening and thinning of hinge and limbs, leading to apparent Class 2 folds. It could also be suggested that, as sills were injected in the sub-surface,

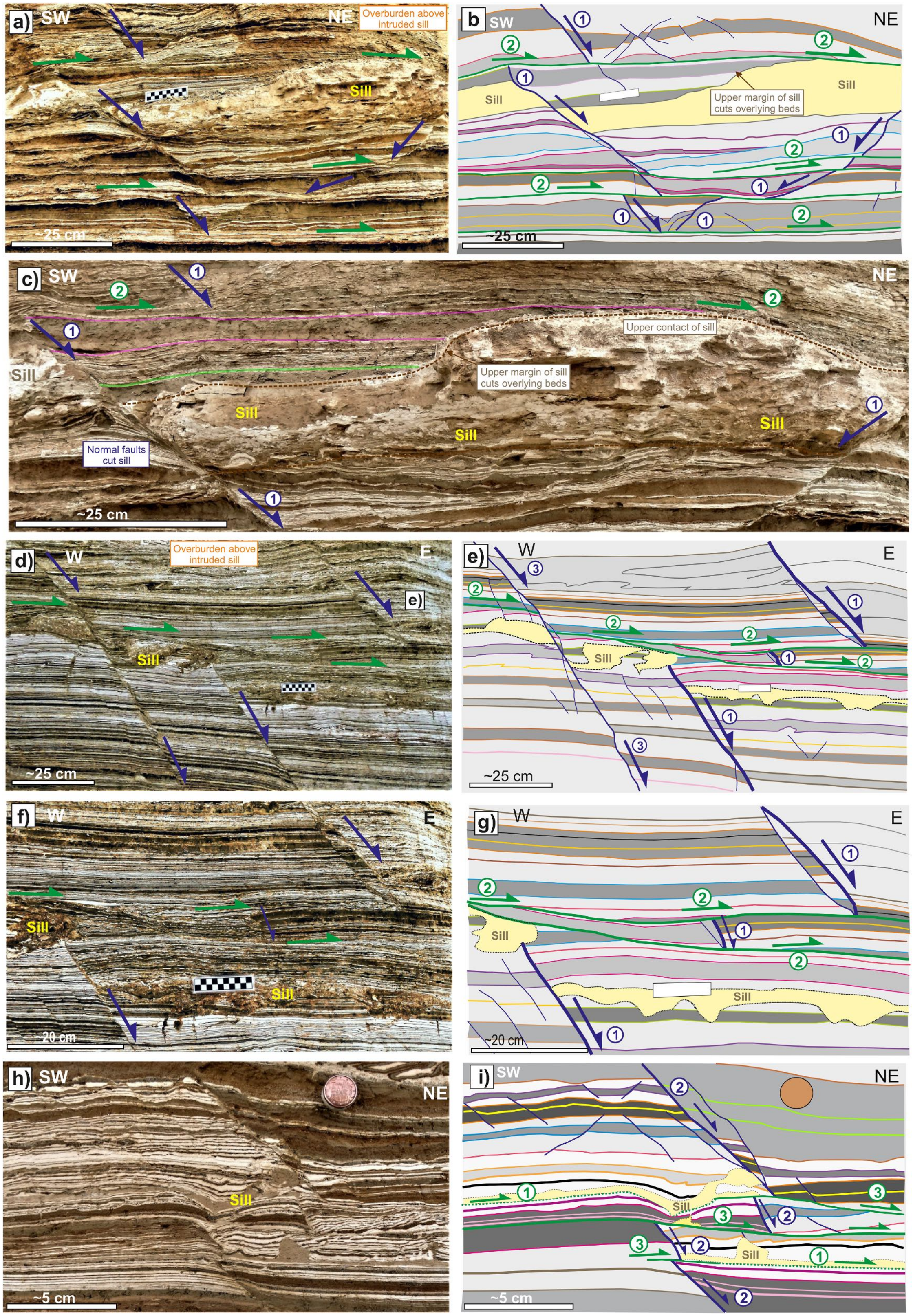


**Fig. 12.** a) Photograph and b) associated line drawing of a sill cross-cutting overlying stratigraphy and being cut by later normal faults. Normal faults (1) define a graben that is displaced by later bed-parallel slip (BPS) (2). c) Detail of sill containing clasts that truncates overlying beds. d) Photograph and e) associated line drawing of a sill formed along a particular stratigraphic level that is subsequently offset across normal faults (1). Later BPS (2) displaces the normal faults, prior to late-stage normal faulting (3) cutting both the sill and BPS (2). f) Close-up photograph and g) associated line drawing provide further detail of the overprinting relationships with normal faults and BPS defining an overall 'sawtooth' geometry. The sill has been remobilised beneath the BPS plane as it locally cuts across the early normal fault (1). h) Photograph and i) associated line drawing of a sill formed along a stratigraphic level that is marked by BPS (1). The sill and BPS (1) are subsequently offset across a normal fault (2) before continued BPS (3). Refer to text for further details.

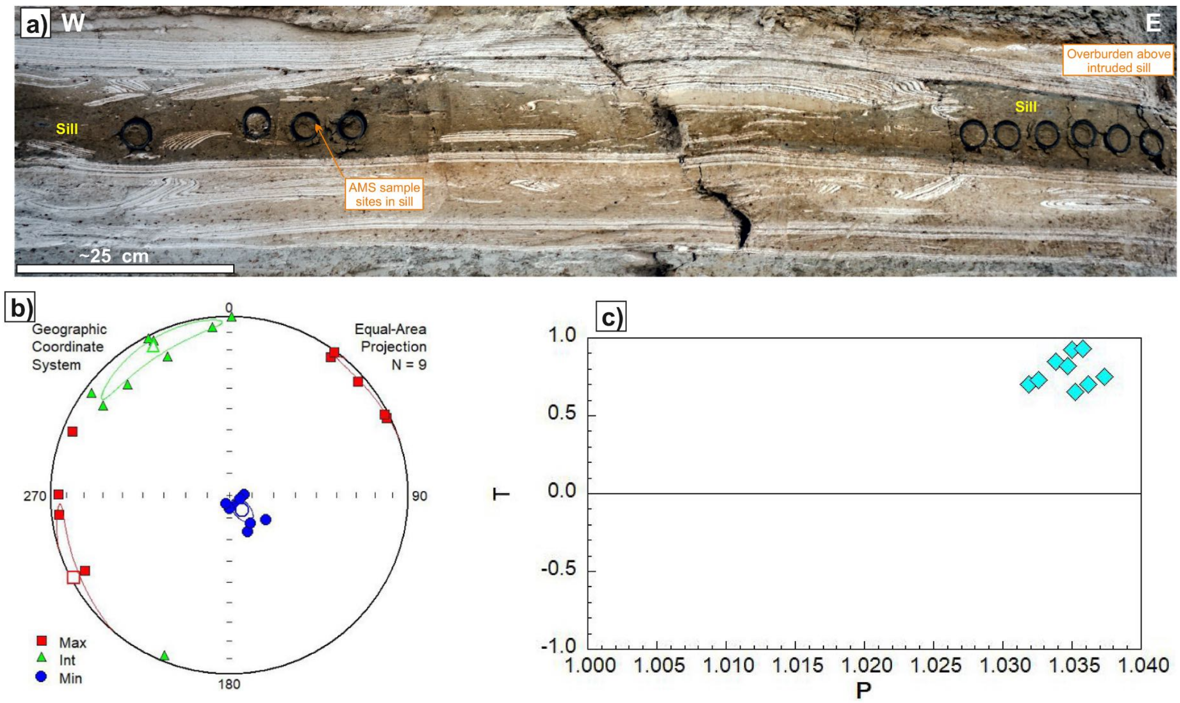


**Fig. 13.** a) Photograph of AMS sample sites (N = 9) within an injected sill shown in Fig. 4a–d b) Lower hemisphere, equal-area projection stereoplot of AMS principal axes with 95% confidence ellipses, and c) *T-P* plot. In AMS stereoplot (b), maximum ($K_1$) axes are shown by red squares, intermediate ($K_2$) axes by green triangles and minimum ($K_3$) axes by blue circles. Refer to text for further details. (For interpretation of the references to colour in this figure legend, the reader is referred to the Web version of this article.)

beds were already slightly more compacted and competent, thereby resulting in the differing fold shapes compared to surficial MTDs.

We suggest that the differing fold geometries adjacent to sills and within MTDs reflect different fold mechanisms (see also Ogata et al., 2014b). Within MTDs, folds initiate by layer-parallel shortening that results in upright buckle folds that are modified by downslope shearing into recumbent tight-isoclinal folds associated with progressive simple shear deformation (Alsop et al., 2020c, their Fig. 6). In peel-back folds, the lower and overturned upper fold limbs are sub-horizontal and parallel to the plane of simple shear. They do not therefore undergo significant deformation and associated reduction in limb thickness. As the bed passes around the hinge it locally becomes vertical and will experience bending due to the horizontal simple shear exerted by the injecting sill. Bending results in local outer arc extension of the bed that creates open fractures injected by the sill (Fig. 6b). Opening of fractures may also be enhanced by later 'flattening' linked to overburden, although this is considered minor. The barb preserved on the tip of the overturned limb is formed during the initial 'rip-up' of the folded horizon and also supports the peel-back fold mechanism.

#### *11.2.2. Why are peel-back folds typically not observed along the upper contacts of sills?*

It is notable that our examples of peel-back folds are only observed along the lower contacts of sedimentary sills (Figs. 6, 7). We also note that sills normally step upwards in the direction of propagation to create 'saucer' shaped intrusions (e.g. Hurst et al., 2011). Stepping in the direction of injection means that flow impacts on the front face of steps along the lower contact, resulting in peel-back folds. Conversely, intrusion along the upper contact of the sill (underside of steps) does not impede flow. Regular upward stepping in the direction of injection is therefore more likely to create peel-back folds along the lower sill contact.

### *11.3. How are folded clasts created within sills?*

Sills frequently inject along beds that are planar and unfolded as this represents an easier path of intrusion compared to cutting across disrupted stratigraphy in folded MTDs. Where sills containing isoclinally folded clasts pass through unfolded and undeformed horizontal beds, the question arises as to where such folded clasts are derived from.

Folded clasts have been described from glacial outwash deposits where soft-sediment clasts were detached from underlying beds and repeatedly folded (Knight, 1999). It is suggested that folding initiated "while part of the underside of the clast … was still attached to the bed." (Knight, 1999, p.301). Clasts are considered to become detached and 'ripped-up' from the bed immediately after folding during turbulent flow. Folding is therefore part of the detachment process of the clast, rather than erosion of a pre-existing folded layer. Folded clasts may thus be considered as portions of peel-back folds that have become detached from the host sediment. Imbrication and folding of mud clasts were also considered by Kawakami and Kawamura (2002, p.180) to form during dragging and displacement by intrastratal flow of sediment. The tight-isoclinal recumbent folds are detached from the host strata and display broadly Class 1B or 1C geometries (Figs. 3a and 6a of Kawakami and Kawamura, 2002). Within the case study we specifically note the following clast attributes.

*Fold styles in clasts* – Although folding within MTDs may create more open and upright buckle folds, there is a general lack of clasts with such open folds in sills. This conundrum is all the greater because numerous clasts within sills define isoclinal folds, the supposed 'end-member' product of progressive deformation. However, the peel-back fold mechanism next to sills will only produce recumbent, isoclinal folds due to the imposed sub-horizontal shear created by sill emplacement and general lack of bed shortening. Such peel-back folds may be detached and incorporated as clasts into the sill. As such, more open or upright folds would not be anticipated to form with this mechanism, although they may be expected where MTDs rework folded sequences.

*Folding of sill fabrics around clasts* – Clasts with isoclinal folds may be detached and are found towards the upper margin of sills (Figs. 4h and 9k) or in beds still attached to host stratigraphy along the lower contact of the sill (Figs. 6, 7). We notice in some cases that aligned aragonite flakes and detrital fragments define a fabric in the sill that is also folded around the tight-isoclinal detached folds (Fig. 4h) and also fold hinges attached to the lower contact (Fig. 6b, e). While fabrics in sills that are folded around attached fold hinges demonstrate that peel-back folding is an integral part of the intrusive process, the preservation of folded fabrics around detached folded clasts indicates a more prolonged phase of deformation and tightening of folds after they became detached.

### *11.3.1. Distinguishing folded clasts in MTDs and sills*

Large, folded clasts and blocks within MTDs may create topography (e.g. Ogata et al., 2014a), which is infilled and draped by overlying sedimentary caps and stratigraphy that is deposited on top of the MTD surface (e.g. Alsop et al., 2020d). Conversely, clasts within sills do not affect the upper intrusive margin of the sill and have no influence on the overlying bedded sequence. In fact, clasts may be truncated and planed flat along the contacts of sills (Fig. 4f).

Within MTDs, angular fragments may contain pre-existing folds that were re-worked from the MTD itself or plucked from the substrate of the MTD. In this case, the clast *contains* folds of varying geometries, with the clast margins cutting across the folds. Conversely, the margins of peel-back fold clasts tend to follow the form of the actual folded surface. This is considered unlikely if clasts are eroded from a folded substrate as the surfaces are too irregular. In summary, clasts within MTDs contain pre-existing folds that are cut across by the clast, whereas folded clasts in sills follow the form of the isoclinal peel-back folds derived from the intrusive margins.

## *11.4. Which criteria help identify bed-parallel sills?*

There have been numerous studies on sandstone injections within deep water marine sequences with Duranti and Hurst (2004, p.18) suggesting a list of criteria for the recognition of sedimentary sills from drill cores, while Hurst et al. (2011) provide a more general overview and catalogue of diagnostic features. Morley et al. (1998) and Morley (2003) provide analyses of mudstone and shale intrusions including sills across a range of scales from both outcrop and seismic data. We summarise the different criteria used to identify sills in Figs. 14 and 15 and now discuss them with respect to the shallow lacustrine sequence of the Dead Sea Basin.

### *11.4.1. External geometry of sills*

The ability of sills to rapidly change thickness when traced laterally along strike has been noted by Hiscott (1979), Kumar and Singh (1982) and Hurst et al. (2011, p.221), amongst others (Figs. 14a and 15a, b). This may lead to blunt or wedge-shaped terminations to sills (e.g. Macdonald and Flecker, 2007) (Fig. 14a). Abrupt changes in sill thickness often develop where irregularities in the upper contact are formed (e.g. Palladino et al., 2020), with Archer (1984) noting localised fracturing over rises in the upper contact. Examples from this study support the marked thickness changes described in sills from other settings and are associated with irregular roof geometries (Fig. 4i and j).

Based on outcrop studies Truswell (1972), Hiscott (1979), Parize and Fries (2003) and Cobain et al. (2015) note that sandstone sills may display changes in stratigraphic position at the scale of the exposure (Fig. 15a and b). The ability to bifurcate and form several segments at different stratigraphic levels is a key characteristic of intrusions that is not shown by depositional units (e.g. Neuwerth et al., 2006; Diggs, 2007; Macdonald and Flecker, 2007; Gao et al., 2020, p.9) (Figs. 3, 14a and 15a, b). Additional geometries that help distinguish sills include bridges and screens of sediment that separate lateral terminations or 'pointed bayonets' of adjacent sills (Figs. 3, 4d and 14a, 15a, b). Bridges, together with bifurcation of sills at different stratigraphic levels, are key geometries that help distinguish sills from depositional units across a range of settings, including bedded lacustrine sequences.

### *11.4.2. Internal structure of sills*

Faint internal banding or layering is a general feature observed within sills (e.g. Figs. 14b and 15a, b) and has been reported by Kawakami and Kawamura (2002), who found it to be better developed if the poorly-sorted sandy matrix contains thin traces or films of mud. Sills up to 20 m thick were studied by Palladino et al. (2020) who note that mm-to dm-thick banding formed parallel to the margins of the sill and possibly represent repeated pulses of injection (e.g. Hurst et al., 2011, p.238). The thickest sills reported by Palladino et al. (2020) also contain convolute laminations and fluid escape structures, suggesting a later phase of fluid expulsion may develop. Similar fluid escape structures are also noted in this study (Fig. 6a, c, f). The development of lamination parallel to contacts is clearly not unique to sills and cannot be used as a diagnostic criterion.

Angular clasts that form breccia within sills have been reported by Archer (1984) (Figs. 14b and 15a, b). Such breccia zones are discontinuous, form lenticular pods, and may also display a jigsaw configuration where adjacent clasts can be fitted back together (e.g. Palladino et al., 2020). The matrix of sills can contain normally graded intervals with coarser grains at the base, or display inverse grading with coarser material towards the top (e.g. Macdonald and Flecker, 2007; Hurst et al., 2011, p.238). Although breccias are observed within sills in the present study (Fig. 4e–g, 14b), no grading is present, suggesting that the clasts and matrix may not have large density or viscosity contrasts, while potentially rapid intrusion leaves little time for organized grain settling. Brecciation and grading form within depositional beds across a range of sedimentary environments and are not unique features that can be used to identify sills. However, if brecciated clasts are unequivocally derived from the overlying sequence, then this strengthens the sill interpretation.

### *11.4.3. Nature of sill contacts*

Sharp upper contacts are a common feature of sills (e.g. Figs. 14c and 15c) that may also be associated with tool marks (e.g. Macdonald and Flecker, 2007) more typically found along the base of turbidites (e.g. Tucker, 2003, p.86). The development of tool marks on upper surfaces is created by the injection of the underlying sill, implying that intrusion was rapid. Rapid intrusion is also indicated by erosion of the overlying sequence, which serves as conclusive evidence that the sill does not form part of a conformable sedimentary sequence (e.g. Diggs, 2007; Palladino et al., 2016) (Figs. 14c and 15c). Both the lower and upper contacts of sills may be erosive and define irregular shapes with respect to the host sediment (e.g. Macdonald and Flecker, 2007; Hurst et al., 2011). Erosion along the upper surface of the sill may cross-cut laminae in overburden above the sill and create convex-up features termed 'scallops' by Hurst et al. (2011, p.221), which can be up to 10's of metres in width (Palladino et al., 2020) (Figs. 1, 14c and 15c). Although scallops in the case study are smaller (<1 m) (Fig. 4a–d), the erosion and cross-cutting of overlying laminae demonstrates the intrusive origin of the sill. The 'frilled' nature of the upper sill contact (Fig. 9e–h) shows that truncations were created by erosion rather than BPS detachments that generate planar surfaces (Alsop et al., 2020a).

Highly irregular erosion may result in isolated roof pendants being locally preserved along the upper surface of sills (e.g. Archer, 1984, p.1203) (Figs. 14c and 15c). In some cases, the 'pendant' may become entirely detached from the roof to create clasts of recognisable overburden stratigraphy within the sill (e.g. Archer, 1984) (Fig. 4g). Such detached roof pendants in sills should not be confused with ball and pillow structures formed in unstably stratified depositional sequences. Other irregularities along sill contacts may be caused by minor apophyses injecting both upwards and downwards from sills resulting in local deflections of laminae, and once again demonstrating the intrusive origin of the sill (Figs. 14c and 15c). The nature of sill contacts, and in

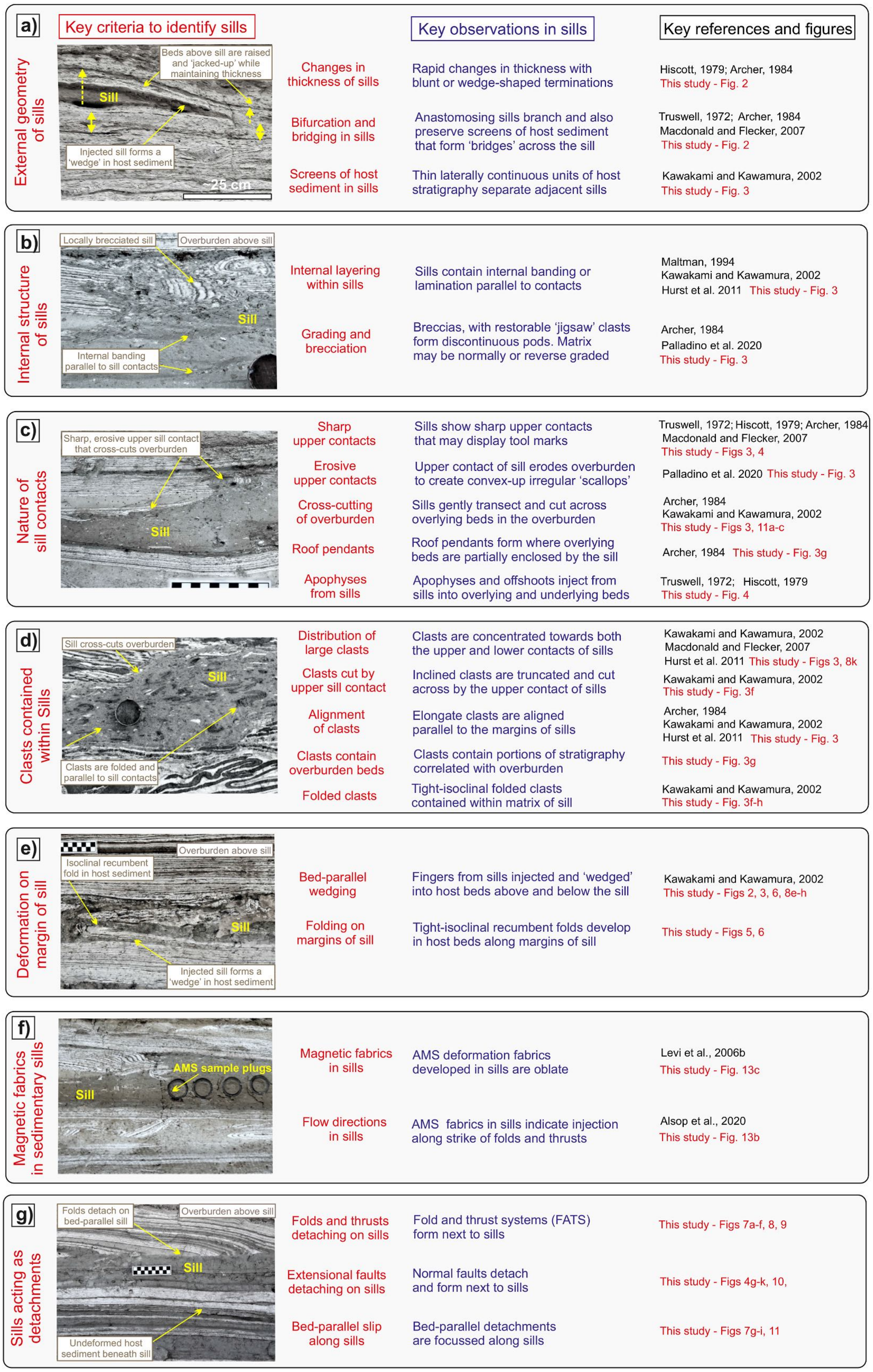


**Fig. 14.** Summary of key criteria, observations, references and figure numbers used in this study to identify sedimentary sills in bedded lacustrine sequences. Distinguishing criteria are based on a) external geometry of sills, b) internal structures of sills, c) nature of sill contacts, d) clasts within sills, e) deformation on margins of sills, f) magnetic fabrics within sills, and g) sills acting as detachments during gravity-driven deformation.

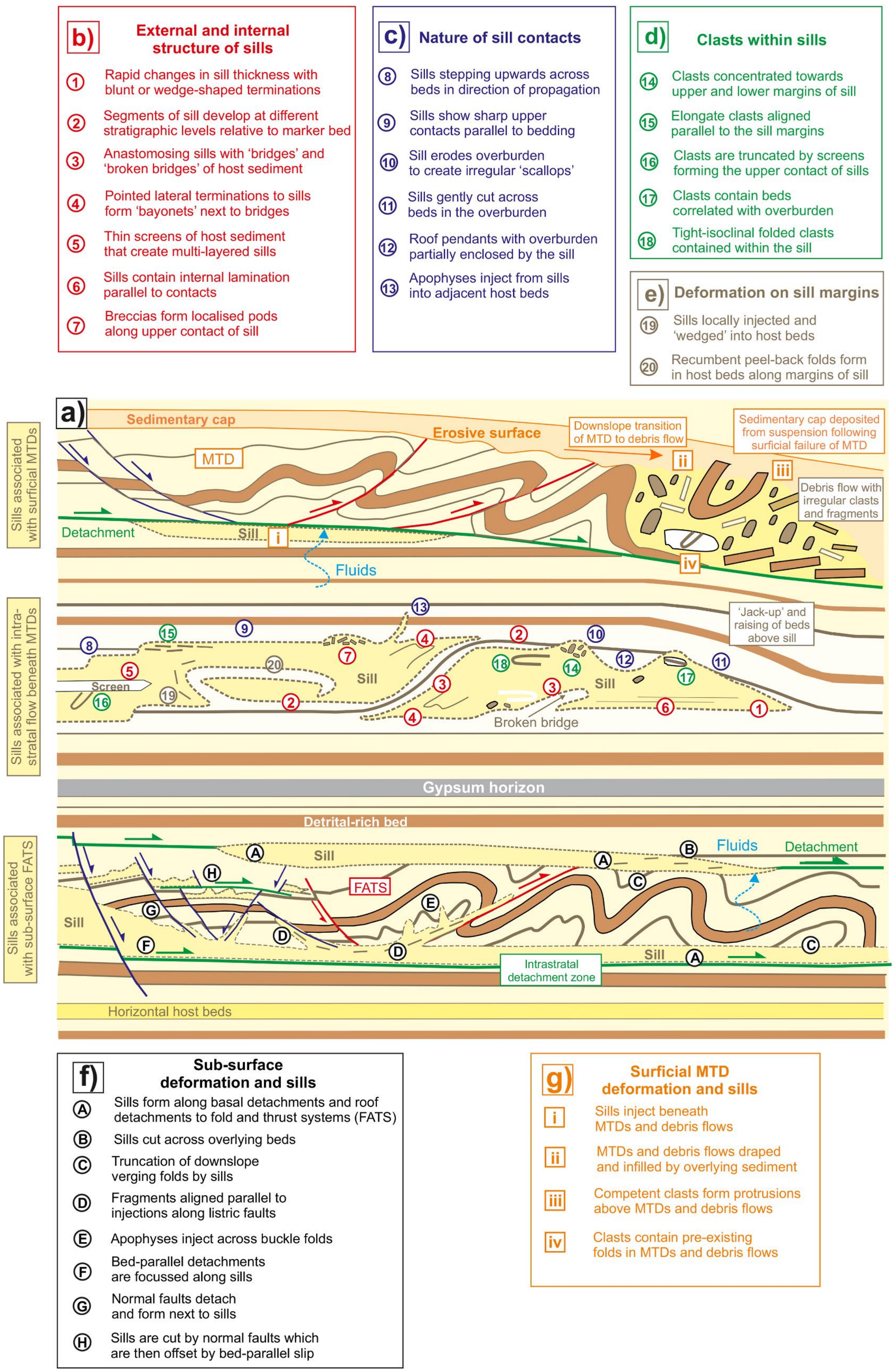


**Fig. 15.** a) Cartoon summarizing sedimentary sills associated with sub-surface fold and thrust systems (FATS), intrastratal flow beneath MTDs and the base of MTDs. Criteria to identify sills in bedded sequences are based on b) external and internal structures of sills (denoted by circled red numbers 1–7), c) nature of sill contacts (circled blue numbers 8–13), d) clasts within sills (circled green numbers 14–18), and e) deformation on margins of sills (circled brown numbers 19–20). Criteria to distinguish f) sills associated with sub-surface deformation (denoted by circled black letters A-H) from g) surficial MTDs and debris flows (boxed orange roman numerals i-iv) are also listed. (For interpretation of the references to colour in this figure legend, the reader is referred to the Web version of this article.)

particular the presence of erosive upper contacts, are a key diagnostic feature of sills (Figs. 14c and 15c).

*11.4.4. Clasts contained within sills*

Clasts have long been recognised to form a significant and identifiable component of sedimentary sills (e.g. Truswell, 1972; Hiscott, 1979; Surlyk et al., 2007; Cobain et al., 2015; Palladino et al., 2016) (Figs. 14d and 15d). In some cases, clasts have been only partially detached from the host sediment (e.g. Kawakami and Kawamura, 2002) thereby suggesting that large clasts are sourced and eroded from the adjacent beds (e.g. Chough and Chun, 1988; Hurst et al., 2011). An alternative interpretation summarised by Cobain et al. (2015) is that clasts are created by sills intruding along anastomosing fractures that preserve unmoved fragments of host rock (or clasts) within them. In the present case study, the lack of fracturing adjacent to sills, coupled with the variably orientated and folded nature of clasts, supports an erosive origin (Fig. 4e–h).

Kawakami and Kawamura (2002, p.175) note that fragmented clasts dominate in the upper part of the sill, while Macdonald and Flecker (2007), Hurst et al. (2011) and Cobain et al. (2015) observe ripped up angular clasts towards both the upper and lower contacts (Figs. 14d and 15d). In the case study, clasts are concentrated towards either the upper (Fig. 9k-m) or lower margins (Fig. 11e–h) of sills. A concentration of clasts towards the upper sill margin suggests that there may have been erosion along this upper contact resulting in the 'rip-down' clasts of Chough and Chun (1988) (Fig. 4d–h). This is opposite to that generally observed in depositional systems where clasts are typically focussed towards the base of the unit, although reverse grading is possible.

Clasts may become aligned due to flow within a sill and this is pronounced where laminated sediment forms elongate clasts that create aligned trains (e.g. Archer, 1984), while mud-clasts form aligned ellipsoidal shapes within sills (Kawakami and Kawamura, 2002) (Figs. 14d and 15d). In the case study, clasts are parallel not only to the margins of sills, but also to the obliquely cross-cutting sheets formed along faults (Fig. 5i). This suggests that sediment injection, rather than settling or later compaction, leads to such fabrics. In summary, clasts originate from a variety of potential processes in sedimentary systems and are not unique to sills. However, where clasts are distributed towards the top of units, or truncated by upper contacts, or contain recognisable stratigraphic units sourced from overburden above the unit, then this significantly strengthens the sill interpretation (Figs. 14d and 15d).

*11.4.5. Folding and deformation on margins of sills*

Recumbent isoclinal folds formed in basal shear zones directly beneath the downslope toe of MTDs have been reported by a number of authors, including Jablonska et al. (2018, their Fig. 12), Sobiesiak et al. (2018, their Fig. 9) and Cardona et al. (2020, their Fig. 13i and j). As recumbent folds are created by substrate shearing induced by both overlying MTDs and sills, resulting folds are superficially similar. However, there are a number of important differences when distinguishing folds developed beneath MTDs from those described from below sills (Figs. 14e and 15e).

Firstly, in the examples noted from beneath MTDs, there is no evidence of sediment injection and 'wedging' beneath the fold, which is observed in sills (Figs. 6, 7). This is the most distinguishing factor between peel-back folds created below MTDs or in substrate beneath sills. Secondly, the characteristic 'fish-hook barb' that forms where the beds are initially ripped up during injection of sills also appears to be missing from the MTD examples, although this could simply reflect different competencies and rates of deformation in the two settings. Thirdly, the vergence of peel-back folds in MTDs is directed downslope parallel to movement, whereas the vergence of peel-back folds beneath sills is in the direction of intrusion, which may be downslope but can also be parallel to the strike of the slope and even upslope in some cases. Thus, peel-back folds are expected to verge towards the termination of the sill rather than necessarily in the downslope direction.

*11.4.6. Magnetic fabrics within sedimentary sills*

AMS may be considered another useful criterion in the identification of sedimentary sills as the deformation fabric of sills is different from the deposition fabric of undisturbed beds. In the case of horizontal injection and formation of sills that enhances weak particle alignment, a 'quasi deformation fabric evolves, in which the oblateness of the AMS ellipsoid is quite strong but $K_1$ and $K_2$ axes are somewhat-clustered and distinguishable (Rees and Woodall, 1975; Levi et al., 2006a). Interpretation of the flow direction is based on $K_3$ inclinations (e.g. Liu et al., 2001) and is in the opposite direction to the inclination of $K_1$ or $K_2$ axes (Levi et al., 2006a). In the case of high flow rates, all three AMS axes are distinguishable and the shape of the AMS ellipsoid changes gradually from oblate ($k_3 \ll k_1, k_2$) to prolate ($k_3, k_2 \ll k_1$). The principal axes are either grouped or streaked-out due to the rotation of particles during fast flow.

In the case study, the direction of injection within the sill is interpreted to be towards the SE (Fig. 13a–c, 14f). The direction of slumping based on structural analysis in the overlying MTD is downslope towards the NE, and the flow within the sill is therefore normal to this and parallel to the inferred strike of the slope. It is also parallel to the strike of overlying thrusts within the MTD (Alsop et al., 2017). Flow and injection of sediment parallel to the strike of overlying thrusts has previously been reported from magnetic fabrics elsewhere in the Lisan Formation (Alsop et al., 2018).

### 11.5. What is the timing and role of sills in gravity-driven deformation?

The relationship between intrusion of sills and gravity-driven deformation has long been recognised with Hiscott (1979, p.2) stating that "slumping may have been instrumental in the initiation of liquefaction and clastic injection", while Macdonald and Flecker (2007, p.260) note that "Zones of abundant intrusive sands are coincident with the high-strain zones". The role of fluids in generating relatively weak layers that encourage downslope movement to create large-scale MTDs has been examined by a number of authors, including Wu et al. (2021) and Gatter et al. (2021).

Theoretically, sills may have a pre-, syn-, or post-kinematic relationships with respect to gravity-driven downslope movement of sediments. In the case study, it is not always possible to accurately determine the timing relationships as sills are intruded into beds that are unaffected by deformation, although regional clastic dykes consistently cross-cut sills, indicating that sills are not a late-stage feature (Fig. 3a–c, 4a-e). In other cases, sills may develop directly along basal detachments along which overlying FATS propagate (Fig. 8a–i, 9a-d, 15f). Sills and associated apophyses inject into the overlying beds indicating that the intrusions were syn-kinematic and that deformation developed below the sediment surface.

Sills may also intrude during extensional deformation where sheets inject along normal faults (Fig. 5g–k, 11i-k), and also along associated bed-parallel detachments (Figs. 11, 14f and 15g). Cross-cutting relationships suggest that in some cases sills develop along bed-parallel detachments that are cut by later normal faults (Fig. 12). Terminations of sills marked by either contractional thrust faults (Fig. 9e–h) or extensional listric fault geometries (Fig. 11e–h) indicates that sediment mobilization and injection of sills occurred during gravity-driven deformation.

In general, the timing of sills with contractional and extensional deformation is broadly contemporaneous. As sills are considered to be geologically instantaneous, due to fluidization or liquefaction being temporary and not maintained over longer periods of time (e.g. Shanmugam, 2020), then associated deformation must also be rapid rather than related to creep processes. These observations support sub-surface sediment mobilization and injection of sills during slumping, with the trigger for fluidization and liquefaction potentially relating to the earthquake that also created the slope failure and deformation of sediment. In summary, sills may either pre-date or be synchronous with gravity-driven downslope deformation (Figs. 14g and 15f). No examples of sills clearly cross-cutting and therefore post-dating deformation have been observed in this study. These observations of mobilised sediments adjacent to downslope verging folds and thrusts suggest that fluid pressures within detrital-rich units were significantly increased during earthquakes and downslope movement of MTDs and slumps, as suggested by Ogata et al. (2014a) and Alsop et al. (2021a).

### *11.6. What are the consequences of misidentifying sills?*

The failure to identify sedimentary sills within lacustrine sequences has a number of implications, not only for the interpretation of the general stratigraphy and depositional facies of a sequence, but also on the effects such sills may have on mechanical stratigraphy during any subsequent deformation of the laminated lake sediments. Remobilization of MTDs leading to sediment injection 'lenses' and volcanoes has previously been recognised using high resolution seismic data in Chilean lakes by Moernaut et al. (2009). These authors further suggest that intrusions may be multi-phase, reflecting repeated earthquake cycles as sediment injections reach higher stratigraphic levels.

#### *11.6.1. Rates of deformation*

As sedimentary intrusions are considered to inject at geologically instantaneous rates, any deformation associated with sills must also be rapid. This supports rapid movement of surficial MTDs and sub-surface FATS rather than downslope creep of the sedimentary pile. However, deformation may continue after the initial intrusion, in which case the sill itself may become deformed, making identification more problematic.

#### *11.6.2. Styles of deformation*

It is critical to distinguish sedimentary sills, intruded in the shallow sub-surface, from turbidites and debris flows, deposited at the surface (Fig. 15f and g). If sills containing fragments and clasts are misidentified as debris flows and MTDs, this may lead to incorrect estimates of styles of deformation and slope failure (see Hurst et al., 2011; Alsop et al., 2022). Kawakami and Kawamura (2002, p.177) provide a list of criteria to distinguish sediment injection and deformation within sills from debris flow deposits. Although sills may display erosive upper contacts with the overlying host sediments, this will not be observed in depositional debris flows (Fig. 15f and g). In addition, while the upper contact of a sill may create an irregular surface that cuts across laminae in the host sediment, depositional beds may drape over and infill underlying irregularities (Fig. 15f and g). Although stratigraphy within overlying host sediments may project downwards into sills to create 'roof pendants', these are not observed in debris flows. Cohesive mud clasts may form protrusions at the surface of debris flows (e.g. Ogata et al., 2020, their Fig. 6), whereas elongate mud clasts within sills are truncated along the upper contact. This stratigraphic signature and relationship with the overlying sequence is key to distinguishing sills containing clasts from debris flows (Fig. 15f and g).

#### *11.6.3. Depths of deformation*

MTDs and FATS generally compact and de-water sediment during movement and therefore form significant heterogeneities in buried sequences that may later focus sedimentary sills. However, where outcrops or observations are limited, as in narrow drill cores, then injection of sills along roof detachments above sub-surface FATS may be confused with sedimentary caps or turbidites deposited from suspension above MTDs (e.g. photo in Fig. 14d). This may lead to a misidentification of the deformed horizon as being surficial rather than sub-surface, with implications for the timing of deformation and earthquakes linked to palaeoseismicity (see Alsop et al., 2022).

## 12. Conclusions

A range of criteria have been suggested to enable recognition of sandstone and mudstone sills in bedded sequences that are generally deep-marine in origin. In this study, we have applied some of these outcrop criteria to lacustrine sequences, where bedding is generally developed on a finer scale and sediment compositions can be significantly different. These criteria are summarised in Figs. 14 and 15. It is important to recognise sedimentary sills in lacustrine sequences, as misidentification of sills and turbidites would compromise the palaeoseismic history where such lacustrine turbidites are regarded as potentially representing major seismic events in the sediment record. We highlight a number of specific conclusions below.

1) Within this case study, sedimentary sills are considered to be created by increases in fluid pressure generated by seismicity that also triggered the slope failure associated with downslope movement of MTDs and FATS.
2) The fluidization and intrusion of sediment injections generated by seismicity and associated MTDs and FATS results in sediment weakening and may further enhance and localize bulk kinematics associated with downslope deformation.
3) Thick detrital beds, MTDs, or units that undergo early cementation (such as gypsum horizons) may act as baffles to fluid flow and thereby locally increase pore fluid pressure. This encourages sills to form and inject directly beneath such baffles.
4) Sills may form along bed-parallel detachments associated with both extensional and contractional deformation. Injection of apophyses to sills along thrust ramps and normal faults suggests that these structures also formed rapidly in the sub-surface.
5) Intrusion of sills results in deformation of adjacent host beds marked by plucking of clasts from the walls of the sill. Injection of sills also creates recumbent 'peel-back' folds in host strata that form through rolling hinge migration, resulting in overturned limbs longer than the thickness of the sill.
6) MTD folds initiate by buckling and are strongly modified by simple shear, whereas peel-back folds are created by simple shear with local bending at the hinge. This may explain why peel-back folds adjacent to sills have Class 1B/1C fold geometries that differ from Class 2 forms in MTDs, despite both being tight-isoclinal and recumbent.
7) Taken in isolation, the most unique features to sills are erosive upper contacts that cut across laminae in the overlying host sediment, together with bifurcation and segmentation of sills that cut across stratigraphy at different levels. In general, we therefore need to use a broad combination of criteria that collectively may be used to identify sills.
8) The application of AMS analysis distinguishes between deposition fabrics in beds and injection or deformation fabric in horizontally injected sills. AMS analysis reveals oblate fabrics with trails of minimum ($K_3$) magnetic susceptibility axes indicating intrusion of sedimentary sills parallel to the strike of the palaeoslope and overlying folds and thrusts.
9) The consequences of mis-identifying sills are that stratigraphic sequences may be misinterpreted and miscorrelated. If sills injected above sub-surface fold and thrust systems are confused with sedimentary caps deposited from suspension, then the true nature of the

sub-surface FATS is missed, with inherent consequences for palaeoseismicity.

## Author statement

G.I. Alsop – Fieldwork, conceptualization, writing, R. Weinberger - Fieldwork, conceptualization, writing, S. Marco - Fieldwork, conceptualization, writing, T. Levi - Fieldwork, conceptualization, writing.

## Declaration of competing interest

The authors declare that they have no known competing financial interests or personal relationships that could have appeared to influence the work reported in this paper.

## Acknowledgements

RW was supported by the Israel Science Foundation (ISF grant No. 868/17). SM acknowledges the Israel Science Foundation (ISF grant No. 1645/19) and the Ministry of National Infrastructures, Energy and Water Resources (grant #214-17-027). TL acknowledges the Israeli government GSI DS project 40706. We thank Fabrizio Agosta for efficient editorial handling, together with two anonymous reviewers who provided constructive comments that helped improve the paper.

## References

Alsop, G.I., Marco, S., Weinberger, R., Levi, T., 2017. Upslope-verging back thrusts developed during downslope-directed slumping of mass transport deposits. J. Struct. Geol. 100, 45–61.
Alsop, G.I., Weinberger, R., Marco, S., 2018. Distinguishing thrust sequences in gravity-driven fold and thrust belts. J. Struct. Geol. 109, 99–119.
Alsop, G.I., Weinberger, R., Marco, S., Levi, T., 2019. Identifying soft-sediment deformation in rocks. J. Struct. Geol. 125, 248–255. https://doi.org/10.1016/j.jsg.2017.09.001.
Alsop, G.I., Weinberger, R., Marco, S., Levi, T., 2020a. Bed-parallel slip: identifying missing displacement in mass transport deposits. J. Struct. Geol. 131, 103952.
Alsop, G.I., Weinberger, R., Marco, S., Levi, T., 2020b. Distinguishing coeval patterns of contraction and collapse around flow lobes in mass transport deposits. J. Struct. Geol. 134, 104013.
Alsop, G.I., Weinberger, R., Marco, S., Levi, T., 2020c. Folding during soft-sediment deformation. In: Bond, C.E., Lebit, H.D. (Eds.), Folding and Fracturing of Rocks: 50 Years since the Seminal Text Book of J.G. Ramsay, vol. 487. Geological Society Special Publication, pp. 81–104. https://doi.org/10.1144/SP487.1.
Alsop, G.I., Weinberger, R., Marco, S., Levi, T., 2020d. Fold and thrust systems in mass transport deposits around the Dead Sea Basin. In: Ogata, K., Festa, A., Pini, G.A. (Eds.), Submarine Landslides: Subaqueous Mass Transport Deposits from Outcrops to Seismic Profiles. American Geophysical Union Monograph Series, vol. 246. John Wiley & Sons Inc. 384pp, ISBN 978-1-119-50058-2, pp. 139–154.
Alsop, G.I., Weinberger, R., Marco, S., Levi, T., 2021a. Detachment fold duplexes within gravity-driven fold and thrust systems. J. Struct. Geol. 142, 104207.
Alsop, G.I., Weinberger, R., Marco, S., Levi, T., 2021b. Criteria to discriminate between different models of thrust ramping in gravity-driven fold and thrust systems. J. Struct. Geol. 150, 104396.
Alsop, G.I., Marco, S., Levi, T., 2022. Recognising surface versus sub-surface deformation of soft-sediments: consequences and considerations for palaeoseismic studies. J. Struct. Geol. 154, 104493.
Ambraseys, N., 1988. Engineering seismology. Earthq. Eng. Struct. Dynam. 17, 1–105.
Archer, J.B., 1984. Clastic intrusions in deep-sea fan deposits of the Rosroe formation, lower Ordovician, western Ireland. J. Sediment. Petrol. 54, 1197–1205.
Arkin, Y., Michaeli, L., 1986. The significance of shear strength in the deformation of laminated sediments in the Dead Sea area. Isr. J. Earth Sci. 35, 61–72.
Auchter, N.C., Romans, B.W., Hubbard, S.M., 2016. Influence of deposit architecture on intrastratal deformation, slope deposits of the Tres Pasos Formation, Chile. Sediment. Geol. 341, 13–26.
Baer, G., 1993. Flow directions in sills and dikes and formation of cauldrons in eastern Makhtesh Ramon. Isr. J. Earth-Sci. 42 (3–4), 133–148 ().
Bartov, Y., Stein, M., Enzel, Y., Agnon, A., Reches, Z., 2002. Lake levels and sequence stratigraphy of Lake lisan, the late Pleistocene precursor of the Dead Sea. Quat. Res. 57, 9–21.
Bartov, Y., Goldstein, S.L., Stein, M., Enzel, Y., 2003. Catastrophic arid episodes in the Eastern mediterranean linked with the North Atlantic Heinrich events. Geol. 31, 439–442.
Begin, Z.B., Ehrlich, A., Nathan, Y., 1974. Lake Lisan, the Pleistocene precursor of the Dead Sea. Geol. Surv. Isr. Bull. 63, 30.
Begin, B.Z., Steinberg, D.M., Ichinose, G.A., Marco, S., 2005. A 40,000 years unchanging of the seismic regime in the Dead Sea rift. Geol. 33, 257–260.
Ben-Dor, Y., Neugebauer, I., Enzel, Y., Schwab, M.J., Tjallingii, R., Erel, Y., Brauer, A., 2019. Varves of the Dead Sea sedimentary record. Quat. Sci. Rev. 215, 173–184.
Borradaile, G.J., Jackson, M., 2004. Anisotropy of magnetic susceptibility (AMS): magnetic petrofabrics of deformed rocks. Geol. Soc. London, Spec. Publ. 238, 299–360. https://doi.org/10.1144/GSL.SP.2004.238.01.18.
Cardona, S., Wood, L.J., Dugan, B., Jobe, Z., Strachan, L.J., 2020. Characterization of the Rapanui mass-transport deposit and the basal shear zone: mount messenger formation, Taranaki basin, New Zealand. Sedimentology 67, 2111–2148. https://doi.org/10.1111/sed.12697.
Chough, S.K., Chun, S.S., 1988. Intrastratal rip-down clasts, late cretaceous Uhangri formation, southwest Korea. J. Sediment. Petrol. 58, 530–533.
Cobain, S.L., Peakall, J., Hodgson, D.M., 2015. Interpretation of propagation direction and relative depth in clastic injectites: implications for laminar versus turbulent flow processes. Geol. Soc. Am. Bull. 127, 1816–1830.
Collinson, J., 1994. Sedimentary deformational structures. In: Maltman, A. (Ed.), The Geological Deformation of Sediments. Chapman & Hall, London, pp. 95–124.
Diggs, T.N., 2007. An outcrop study of clastic-injection structures in the Carboniferous Tesnus Formation, Marathon basin, Trans-Pecos Texas. In: Hurst, A., Cartwright, J. (Eds.), Sand Injectites: Implications for Hydrocarbon Exploration and Production. American Association of Petroleum Geologists Memoir, Tulsa, pp. 209–219.
Diller, J.S., 1890. Sandstone Dikes, vol. 1. Geological Society of America Bulletin, pp. 411–442.
Dixon, R.J., Schofield, K., Anderton, R., Reynolds, A.D., Alexander, R.W.S., Williams, M.C., Davies, K.G., 1995. Sandstone diapirism and clastic intrusion in the Tertiary submarine fans of the Bruce-Beryl Embayment, Quadrant 9, UKCS. In: Hartley, A.J., Prosser, D.J. (Eds.), Characterisation of Deep-Marine Clastic Systems: Special Publication, vol. 94. Geological Society, London, pp. 77–94.
Duffield, W.A., Bacon, C.R., Delaney, P.T., 1986. Deformation of poorly consolidated sediment during shallow emplacement of a basalt sill, Coso Range, California. Bull. Volcanol. 48, 97–107.
Duranti, D., Hurst, A., 2004. Fluidisation and injection in the deep-water sandstones of the Eocene Alba formation (UK North sea). Sedimentology 51, 503–531.
El-Isa, Z.H., Mustafa, H., 1986. Earthquake deformations in the Lisan deposits and seismotectonic implications. Geophys. J. Roy. Astron. Soc. 86, 413–424.
Fossen, H., 2016. Structural Geology, second ed. Cambridge University Press, Cambridge, UK, p. 510.
Frydman, S., Charrach, J., Goretsky, I., 2008. Geotechnical properties of evaporite soils of the Dead Sea area. Eng. Geol. 101, 236–244.
Gao, Y., Jiang, Z., Best, J.L., Zhang, J., 2020. Soft-sediment deformation structures as indicators of tectono-volcanic activity during evolution of a lacustrine basin: a case study from the Upper Triassic Ordos Basin, China. Mar. Petrol. Geol. 115, 104250.
Gatter, R., Clare, M.A., Kuhlmann, J., Huhn, K., 2021. Characterisation of weak layers, physical controls on their global distribution and their role in submarine landslide formation. Earth Sci. Rev. 223, 103845.
Haase-Schramm, A., Goldstein, S.L., Stein, M., 2004. U-Th dating of Lake Lisan aragonite (late Pleistocene Dead Sea) and implications for glacial East Mediterranean climate change. Geochem. Cosmochim. Acta 68, 985–1005.
Haliva-Cohen, A., Stein, M., Goldstein, S.L., Sandler, A., Starinsky, A., 2012. Sources and transport routes of fine detritus material to the late Quaternary Dead Sea basin. Quat. Sci. Rev. 50, 55–70.
Hiscott, R.N., 1979. Clastic sills and dikes associated with deep-water sandstones, Tourelle Formation, Ordovician, Quebec. J. Sediment. Petrol. 49, 1–10.
Hurst, A., Cartwright, J., Huuse, M., Duranti, D., 2007. Sand injectites in deep-water clastic reservoirs: are they there and do they matter? Paper 120. AAPG Studies in Geology. In: Nilsen, T.H., Shaw, R.D., Steffans, G.S., Studlick, J.R.J. (Eds.), Atlas of Deepwater Outcrops, vol. 56. CD-Rom, p. 24p.
Hurst, A., Scott, A., Vigorito, M., 2011. Physical characteristics of sand injectites. Earth Sci. Rev. 106, 215–246.
Hutton, D.H.W., 2009. Insights into magmatism in volcanic margins: bridge structures and a new mechanism of basic sill emplacement – Theron Mountains, Antarctica. Petrol. Geosci. 15, 269–278.
Ichinose, G.A., Begin, Z.B., 2004. Simulation of Tsunamis and Lake Seiches for the Late Pleistocene Lake Lisan and the Dead Sea. Geological Survey of Israel Report GSI/7/04, p. 50.
Jablonska, D., Di Celma, C., Tondi, E., Alsop, G.I., 2018. Internal architecture of mass-transport deposits in basinal carbonates: a case study from southern Italy. Sedimentology 65, 1246–1276. https://doi.org/10.1111/sed.12420.
Jacoby, Y., Weinberger, R., Levi, T., Marco, S., 2015. Clastic dikes in the Dead Sea basin as indicators of local site amplification. Nat. Hazards 75 (2), 1649–1676 ().
Jelinek, V., 1978. Statistical processing of anisotropy of magnetic susceptibility measured on group of specimen. Studia Geophys. Geod. 22, 50–62.
Jelínek, V., 1981. Characterization of the magnetic fabric of rocks. Tectonophysics 79, 63–67.
Jenkins, O.P., 1930. Sandstone dikes as conduits for oil migration through shales. AAPG (Am. Assoc. Pet. Geol.) Bull. 14, 411–421.
Kagan, E.J., Stein, M., Marco, S., 2018. Integrated palaeoseismic chronology of the last glacial Lake Lisan: from lake margin seismites to deep-lake mass transport deposits. J. Geophys. Res. Solid Earth 123 (4), 2806–2824.
Kawakami, G., Kawamura, M., 2002. Sediment flow and deformation (SFD) layers: evidence for intrastratal flow in laminated muddy sediments of the Triassic Osawa Formation, northeast Japan. J. Sediment. Res. 72, 171–181.
Ken-Tor, R., Agnon, A., Enzel, Y., Marco, S., Negendank, J.F.W., Stein, M., 2001. High-resolution geological record of historic earthquakes in the Dead Sea basin. J. Geophys. Res. 106, 2221–2234.

Knight, J., 1999. Morphology and palaeoenvironmental interpretation of deformed soft-sediment clasts: examples from within Late Pleistocene glacial outwash, Tempo Valley, Northern Ireland. Sediment. Geol. 128, 293–306.
Knipe, R.J., 1986. Deformation mechanism path diagrams for sediments undergoing lithification. Mem. Geol. Soc. Am. 166, 151–160.
Kumar, S., Singh, T., 1982. Sandstone dykes in Siwalik sandstone – sedimentology and basin analysis – Subansiri district (Nefa), eastern Himalaya. Sediment. Geol. 33, 217–236.
Leeder, M., 1987. Sediment deformation structures and the palaeotectonic analysis of sedimentary basins, with a case-study from the Carboniferous of northern England. In: Jones, M.E., Preston, R.M.F. (Eds.), Deformation of Sediments and Sedimentary Rocks, vol. 29. Geological Society of London, Special Publication, London, UK, pp. 137–146.
Leila, M., El Sharawy, M., Mohamed, A., Gorini, C., Gioa Bucci, M., Radwan, A.E., Moretti, M., 2022. Soft-sediment deformation structures in the late messinian Abu madi formation, onshore nile delta, Egypt: triggers and tectonostratigraphic implications. Geol. J. https://doi.org/10.1002/gj.4412.
Levi, T., Weinberger, R., Aïfa, T., Eyal, Y., Marco, S., 2006a. Injection mechanism of clay-rich sediments into dikes during earthquakes. G-cubed 7 (12). https://doi.org/10.1029/2006GC001410. Q12009.
Levi, T., Weinberger, R., Aïfa, T., Eyal, Y., Marco, S., 2006b. Earthquake-induced clastic dikes detected by anisotropy of magnetic susceptibility. Geol. 34 (2), 69–72.
Levi, T., Weinberger, R., Eyal, Y., Lyakhovsky, V., Heifetz, E., 2008. Velocities and driving pressures of clay-rich sediments injected into clastic dykes during earthquakes. Geophys. J. Int. 175 (3), 1095–1107 ().
Levi, T., Weinberger, R., Eyal, Y., 2011. A coupled fluid-fracture approach to propagation of clastic dikes during earthquakes. Tectonophysics 498 (1–4), 35–44 ().
Levi, T., Weinberger, R., Marco, S., 2014. Magnetic fabrics induced by dynamic faulting reveal damage zone sizes in soft rocks, Dead Sea basin. Geophys. J. Int. 199 (2), 1214–1229.
Levi, T., Weinberger, R., Alsop, G.I., Marco, S., 2018. Characterizing seismites with anisotropy of magnetic susceptibility. Geol. 46, 827–830.
Liu, B., Saito, Y., Yamazaki, T., Abdeldayem, A., Oda, H., Hori, K., Zhao, Q., 2001. Paleocurrent analysis for the Late Pleistocene–Holocene incised-valley fill of the Yangtze delta, China by using anisotropy of magnetic susceptibility data. Mar. Geol. 176 (1–4), 175–189 ().
Lu, Y., Waldmann, N., Alsop, G.I., Marco, S., 2017. Interpreting soft sediment deformation and mass transport deposits as seismites in the Dead Sea depocenter. J. Geophys. Res. Solid Earth 122, 8305–8325.
Lu, Y., Marco, S., Wetzler, N., Fang, X., Alsop, G.I., Hubert-Ferrari, A., 2021a. A paleoseismic record spanning 2-Myr reveals episodic late Pliocene deformation in the western Qaidam Basin, NE Tibet. Geophys. Res. Lett. 48, e2020GL090530 https://doi.org/10.1029/2020GL090530.
Lu, Y., Moernaut, J., Waldmann, N., Bookman, R., Alsop, G.I., Hubert-Ferrari, A., Strasser, M., Wetzler, N., Agnon, A., Marco, S., 2021b. Orbital- and millennial-scale changes in lake levels facilitate earthquake-triggered mass failures in the Dead Sea Basin. Geophys. Res. Lett. 48 (14), e2021GL093391 https://doi.org/10.1029/2021GL093391.
Lu, Y., Moernaut, J., Bookman, R., Waldmann, N., Wetzler, N., Agnon, A., Marco, S., Alsop, G.I., Strasser, M., Hubert-Ferrari, A., 2021c. A new approach to constrain the seismic origin for prehistoric turbidites as applied to the Dead Sea Basin. Geophys. Res. Lett. 48, e2020GL090947 https://doi.org/10.1029/2020GL090947.
Macdonald, D., Flecker, R., 2007. Injected sand sills in a strike-slip fault zone: a case study from the Pil'sk Suite (Miocene), Southeast Schmidt Peninsula, Sakhalin. In: Hurst, A., Cartwright, J. (Eds.), Sand Injectites: Implications for Hydrocarbon Exploration and Production: AAPG Memoir 87, pp. 253–263.
Magee, C., Muirhead, J., Schofield, N., Walker, R.J., Galland, O., Holford, S., Spacapan, J., Jackson, C.A.-L., McCarthy, W., 2019. Structural signatures of igneous sheet intrusion propagation. J. Struct. Geol. 125, 148–154.
Maltman, A., 1994a. Introduction and overview. In: Maltman, A. (Ed.), The Geological Deformation of Sediments. Chapman & Hall, London, pp. 1–35.
Maltman, A., 1994b. Deformation structures preserved in rocks. In: Maltman, A. (Ed.), The Geological Deformation of Sediments. Chapman & Hall, London, pp. 261–307.
Maltman, A.J., Bolton, A., 2003. How sediments become mobilized. In: Van Rensbergen, R., Hillies, R.R., Maltman, A.J., Morley, C.K. (Eds.), Subsurface Sediment Mobilization, vol. 216. Geological Society, London, Special Publications, pp. 9–20.
Marco, S., Stein, M., Agnon, A., Ron, H., 1996. Long term earthquake clustering: a 50,000 year paleoseismic record in the Dead Sea Graben. J. Geophys. Res. 101, 6179–6192.
Marco, S., Hartal, M., Hazan, N., Lev, L., Stein, M., 2003. Archaeology, history, and geology of the A.D. 749 earthquake, Dead Sea transform. Geol. 31, 665–668.
Migowski, C., Agnon, A., Bookman, R., Negendank, J.F.W., Stein, M., 2004. Recurrence pattern of Holocene earthquakes along the Dead Sea transform revealed by varve-counting and radiocarbon dating of lacustrine sediments. Earth Planet Sci. Lett. 222, 301–314.
Moernaut, J., De Batist, M., Heirman, K., van Daele, M., Pino, M., Brummer, R., Urrutia, R., 2009. Fluidization of buried mass-wasting deposits in lake sediments and its relevance for paleoseismology: results from a reflection seismic study of lakes Villarrica and Calafquen (South-Central Chile). Sediment. Geol. 213, 121–135.
Morley, C.K., Crevello, P., Zulkifli, Haji Ahmad, 1998. Shale tectonics and deformation associated with active diapirism: the Jerudong Anticline, Brunei Darussalam. J. Geol. Soc. 155, 475–490. London.
Morley, C.K., 2003. Outcrop examples of mudstone intrusions from the Jerudong anticline, Brunei Darussalam and inferences for hydrocarbon reservoirs. In: Van Rensbergen, R., Hillies, R.R., Maltman, A.J., Morley, C.K. (Eds.), Subsurface Sediment Mobilization, vol. 216. Geological Society, London, Special Publications, pp. 381–394.
Neuwerth, R., Suter, F., Guzman, C.A., Gorin, G.E., 2006. Soft-sediment deformation in a tectonically active area: the Plio-Pleistocene Zarzal formation in the Cauca valley (western Colombia). Sediment. Geol. 186, 67–88.
Newsome, J.F., 1903. Clastic dikes. Geol. Soc. Am. Bull. 14, 227–268.
Nuriel, P., Weinberger, R., Kylander-Clark, A.R.C., Hacker, B.R., Cradock, J.P., 2017. The onset of the Dead Sea transform based on calcite age-strain analyses. Geol. 45, 587–590.
Obermeier, S.F., 1996. Use of liquefaction-induced features for palaeoseismic analysis– an overview of how seismic liquefaction features can be distinguished from other features and how their regional distribution and properties of source sediment can be used to infer the location and strength of Holocene paleo-earthquakes. Geol. 44, 1–76.
Obermeier, S.F., 2009. Using liquefaction-induced and other soft-sediment features for paleoseismic analysis. Int. Geophys. 95, 497–564. https://doi.org/10.1016/S0074-6142(09)95007-0.
Ogata, K., Mountjoy, J.J., Pini, G.A., Festa, A., Tinterri, E., 2014a. Shear zone liquefaction in mass transport deposit emplacement: a multi-scale integration of seismic reflection and outcrop data. Mar. Geol. 356, 50–64.
Ogata, K., Pogacnik, Z., Pini, G.A., Tunis, G., Festa, A., Camerlenghi, A., Rebesco, M., 2014b. The carbonate mass transport deposits of the Palaeogene Friuli Basin (Italy/Slovenia): internal anatomy and inferred genetic processes. Mar. Geol. 356, 88–110.
Ogata, K., Festa, A., Pini, G.A., Alonso, J.L., 2020. Submarine landslide deposits in orogenic belts: Olistostromes and sedimentary melanges. In: Ogata, K., Festa, A., Pini, G.A. (Eds.), Submarine Landslides: Subaqueous Mass Transport Deposits from Outcrops to Seismic Profiles. American Geophysical Union Monograph Series, vol. 246. John Wiley & Sons Inc. 384pp, pp. 1–26.
Ogawa, Y., 2019. Conceptual consideration and outcrop interpretation on early stage deformation of sand and mud in accretionary prisms for chaotic deposit formation. Gondwana Res. 74, 31–50.
Ortner, H., 2007. Styles of soft-sediment deformation on top of a growing fold system in the Gosau Group at Muttekopf, Northern Calcareous Alps, Austria: slumping versus tectonic deformation. Sediment. Geol. 196, 99–118.
Palladino, G., Grippa, A., Bureau, D., Alsop, G.I., Hurst, A., 2016. Emplacement of sandstone intrusions during contractional tectonics. J. Struct. Geol. 89, 239–249.
Palladino, G., Alsop, G.I., Grippa, A., Zvirtes, G., Phillip, R.P., Hurst, A., 2018. Sandstone-filled normal faults: a case study from Central California. J. Struct. Geol. 110, 86–101.
Palladino, G., Rizzo, R.E., Zvirtes, G., Grippa, A., Phillip, R.P., Healy, D., Alsop, G.I., 2020. Multiple episodes of sand injection leading to accumulation and leakage of hydrocarbons along the San Andreas/San Gregorio fault system, California. Mar. Petrol. Geol. 118, 104431.
Parés, J.M., 2015. Sixty years of anisotropy of magnetic susceptibility in deformed sedimentary rocks. Front. Earth Sci. 3, 4.
Parize, O., Fries, G., 2003. The Vocontian clastic dykes and sills: a geometric model. In: Van Rensebergen, P., Hillis, R.R., Maltman, A.J., Morley, C.K. (Eds.), Subsurface Sediment Mobilization, Geol. Soc. Spec. Publ, vol. 216. Geological Society of London, London, pp. 51–71.
Phillips, E., Lipka, E., van der Meer, J.J.M., 2013. Micromorphological evidence of liquefaction, injection and sediment deposition during basal sliding of glaciers. Quat. Sci. Rev. 81, 114–137.
Porat, N., Levi, T., Weinberger, R., 2007. Possible resetting of quartz OSL signals during earthquakes – evidence from late Pleistocene injection dikes, Dead Sea basin, Israel. Quat. Geochronol. 272–277.
Potter, P.E., Pettijohn, F.J., 1977. Deformational structures up to 1963. In: Paleocurrents and Basin Analysis. Springer, Berlin, Heidelberg. https://doi.org/10.1007/978-3-642-61887-1_10.
Prasad, S., Negendank, J.F.W., Stein, M., 2009. Varve counting reveals high resolution radiocarbon reservoir age variations in palaeolake Lisan. J. Quat. Sci. 24, 690–696.
Ramsay, J.G., 1967. Folding and Fracturing of Rocks. McGraw-Hill, New York, p. 568pp.
Rees, A.I., Woodall, W.A., 1975. The magnetic fabric of some laboratory-deposited sediments. Earth Planet Sci. Lett. 25, 121–130.
Ron, H., Nowaczyk, N.R., Frank, U., Marco, S., McWilliams, M.O., 2006. Magnetic properties of Lake Lisan and Holocene Dead Sea sediments and the fidelity of chemical and detrital remanent magnetization. New frontiers in Dead Sea paleoenvironmental research 401, 171 ().
Rowley, P.J., Kokelaar, P., Menzies, M., Waltham, D., 2011. Shear-derived mixing in dense granular flows. J. Sediment. Res. 81, 874–884.
Schofield, N.J., Brown, D.J., Magee, C., Stevenson, C.T., 2012. Sill morphology and comparison of brittle and non-brittle emplacement mechanisms. J. Geol. Soc. 169, 127–141.
Schwehr, K., Tauxe, L., 2003. Characterization of soft sediment deformation: detection of cryptoslumps using magnetic methods. Geol. 31, 203–206.
Shanmugam, G., 2020. Gravity flows: types, definitions, origins, identification markers, and problems. J. Indian Assoc. Sedimentol. 37, 61–90.
Sneh, A., Weinberger, R., 2014. Major Structures of Israel and Environs, Scale 1:50,000. Israel Geological Survey, Jerusalem.
Sobiesiak, M., Kneller, B.C., Alsop, G.I., Milana, J.P., 2018. Styles of basal interaction beneath mass transport deposits. Mar. Petrol. Geol. 98, 629–639.
Spacapan, J.B., Galland, O., Leanza, H.A., Planke, S., 2017. Igneous sill and finger emplacement mechanism in shaledominated formations: a field study at Cuesta del Chihuido, Neuquén Basin, Argentina. J. Geol. Soc. 174, 422–433.
Strachan, L.J., 2002. Slump-initiated and controlled syndepositional sandstone remobilization: an example from the Namurian of County Clare, Ireland. Sedimentology 49, 25–41.

Surlyk, F., Gjelberg, J., Noe-Nygaard, N., 2007. The upper Jurassic Hareelv formation of east Greenland: a giant sedimentary injection complex. In: Hurst, A., Cartwright, J.A. (Eds.), Sand Injectites: Implications for Hydrocarbon Exploration and Production. American Association of Petroleum Geologists Memoir, Tulsa, pp. 141–149.
Tarling, D., Hrouda, F. (Eds.), 1993. Magnetic Anisotropy of Rocks. Springer Science and Business Media.
Torfstein, A., Goldstein, S.L., Kagan, E., Stein, M., 2013. Integrated multi-site U-Th chronology of the last glacial Lake Lisan. Geochem. Cosmochim. Acta 104, 210–231.
Törő, B., Pratt, B.R., 2015a. Eocene paleoseismic record in the Green River Formation, Fossil Basin, Wyoming — implications of synsedimentary deformation structures in lacustrine carbonate mudstones. J. Sediment. Res. 85, 855–884.
Törő, B., Pratt, B.R., 2015b. Characteristics and implications of sedimentary deformation features in the green river formation (Eocene) in Utah and Colorado. In: Vanden Berg, M.D., Ressetar, R., Birgenheier, L.P. (Eds.), Geology of Utah's Uinta Basin and Uinta Mountains, vol. 45. Utah Geological Association Publication, pp. 371–422.
Törő, B., Pratt, B.R., 2016. Sedimentary record of seismic events in the Eocene Green River Formation and its implications for regional tectonics on lake evolution (Bridger Basin, Wyoming). Sediment. Geol. 344, 175–204.
Truswell, J.F., 1972. Sandstone sheets and related intrusions from Coffee Bay, Transkel, South Africa. J. Sediment. Petrol. 42, 578–583.
Tucker, M.E., 2003. Sedimentary Rocks in the Field, third ed. John Wiley & Sons, Chichester, England, ISBN 0-470-85123-6, p. 244pp.
Weinberger, R., Levi, T., Alsop, G.I., Eyal, Y., 2016. Coseismic horizontal slip revealed by sheared clastic dikes in the Dead Sea basin. Geol. Soc. Am. Bull. 128, 1193–1206.
Weinberger, R., Levi, T., Alsop, G.I., Marco, S., 2017. Kinematics of mass transport deposits revealed by magnetic fabrics. Geophys. Res. Lett. 5807–5817. https://doi.org/10.1002/2017GL072584.
Weinberger, R., Alsop, G.I., Levi, T., 2022. Magnetic fabrics as strain markers in folded soft-sediment layers. J. Struct. Geol. 155, 1–15.
Wu, N., Jackson, C.A.L., Johnson, H.D., Hodgson, D.M., Clare, M.A., Nugraha, H.D., Li, W., 2021. The formation and implications of giant blocks and fluid escape structures in submarine lateral spreads. Basin Res. https://doi.org/10.1111/bre.12532.